Sonochemical Synthesis of Gd^{3+} doped $CoFe_2O_4$ Spinel Ferrite Nanoparticles and Its Physical Properties

Raghvendra Singh Yadav, Ivo Kuřitka, Jarmila Vilcakova, Jaromir Havlica, Lukas Kalina, Pavel Urbánek, Michal Machovsky, David Skoda, Milan Masař, Martin Holek

PII: S1350-4177(17)30378-4
DOI: http://dx.doi.org/10.1016/j.ultsonch.2017.08.024
Reference: ULTSON 3829

To appear in: *Ultrasonics Sonochemistry*

Received Date: 25 July 2017
Revised Date: 22 August 2017
Accepted Date: 23 August 2017

Please cite this article as: R.S. Yadav, I. Kuřitka, J. Vilcakova, J. Havlica, L. Kalina, P. Urbánek, M. Machovsky, D. Skoda, M. Masař, M. Holek, Sonochemical Synthesis of Gd^{3+} doped $CoFe_2O_4$ Spinel Ferrite Nanoparticles and Its Physical Properties, *Ultrasonics Sonochemistry* (2017), doi: http://dx.doi.org/10.1016/j.ultsonch.2017.08.024

Sonochemical Synthesis of Gd^{3+} doped $CoFe_2O_4$ Spinel Ferrite Nanoparticles and Its Physical Properties

Raghvendra Singh Yadav[1]*, Ivo Kuřitka[1], Jarmila Vilcakova[1], Jaromir Havlica[2], Lukas Kalina[2], Pavel Urbánek[1], Michal Machovsky[1], David Skoda[1], Milan Masař[1], Martin Holek[1]

[1]Centre of Polymer Systems, University Institute, Tomas Bata University in Zlín, Trida Tomase Bati 5678, 760 01 Zlín, Czech Republic

[2]Materials Research Centre, Brno University of Technology, Purkyňova 464/118, 61200 Brno, Czech Republic.

*Corresponding Author: E-mail: yadav@utb.cz, raghvendra.nac@gmail.com

Abstract

In this work, a facile and green method for gadolinium doped cobalt ferrite ($CoFe_{2-x}Gd_xO_4$; x=0.00, 0.05, 0.10, 0.15, 0.20) nanoparticles by using ultrasonic irradiation was reported. The impact of Gd^{3+} substitution on the structural, magnetic, dielectric and electrical properties of cobalt ferrite nanoparticles was evaluated. The sonochemically synthesized spinel ferrite nanoparticles were characterized by X-ray Diffraction (XRD), scanning electron microscopy (SEM), Raman spectroscopy, Fourier transform infrared (FTIR) spectroscopy, X-ray photoelectron spectroscopy (XPS), vibrating sample magnetometer (VSM). X-ray diffraction (XRD) study confirmed the formation of single phase spinel ferrite of $CoFe_{2-x}Gd_xO_4$ nanoparticles. XRD results also revealed that ultrasonic irradiation seems to be favourable to achieve highly crystalline single crystal phase gadolinium doped cobalt ferrite nanoparticles without any post annealing process. Fourier Transform Infrared and Raman Spectra confirmed the formation of spinel ferrite crystal structure. X-ray photoelectron spectroscopy revealed the impact of Gd^{3+} substitution in $CoFe_2O_4$ nanoparticles on cation distribution at the tetrahedral and octahedral site in spinel ferrite crystal system. The electrical properties showed that the Gd^{3+} doped cobalt ferrite ($CoFe_{2-x}Gd_xO_4$; x= 0.20) exhibit enhanced

dielectric constant (277 at 100 Hz) and ac conductivity (20.2 x 10^{-9} S/cm at 100 Hz). The modulus spectroscopy demonstrated the impact of Gd^{3+} substitution in cobalt ferrite nanoparticles on grain boundary relaxation time, capacitance and resistance. Magnetic property measurement revealed that the coercivity decreases with Gd^{3+} substitution from 234.32 Oe (x=0.00) to 12.60 Oe (x=0.05) and further increases from 12.60 Oe (x=0.05) to 68.62 Oe (x=0.20). Moreover, saturation magnetization decreases with Gd^{3+} substitution from 40.19 emu/g (x=0.00) to 21.58 emu/g (x=0.20). This work demonstrates that the grain size and cation distribution in Gd^{3+} doped cobalt ferrite nanoparticles synthesized by sonochemical method, is effective in controlling the structural, magnetic, and electrical properties, and can be find very promising applications.

Keywords: Sonochemical Synthesis, Cavitation, Nanoparticles, Magnetic Property, Dielectric Property, Impedance and Modulus Spectroscopy

1. Introduction

Spinel ferrite nanoparticles have a vast potential for several scientific and technological applications **[1-3].** It has application in solar cells, magnetostrictive sensors, transducers, actuators, supercapacitors, Li-ion batteries, drug delivery, hyperthermia, memory devices, microwave and spintronic devices, catalysis, gas sensor, etc. **[4-8].** Among the spinel ferrites, $CoFe_2O_4$ is one of the most applicable ferromagnetic materials which have unique properties such as high coercivity, moderate saturation magnetization, high magneto crystalline anisotropy, high curie temperature, high mechanical and chemical stability **[9-11]**. The physical properties of $CoFe_2O_4$ spinel ferrite nanoparticles depend on grain size and cation distribution at tetrahedral and octahedral sites in spinel ferrite nanoparticles **[12-13]**.

Recently, rare earth ions substituted spinel ferrite nanoparticles has emerged as a promising strategy to improve their physical properties **[14-15]**. The physical properties of spinel ferrite nanoparticles also depend upon the synthesis techniques. Spinel ferrite nanoparticles are synthesized by several chemical synthesis techniques such as co-precipitation method, hydrothermal method,

solvothermal method, micro-emulsion method, sol-gel auto-combustion method, etc. **[16-18]**. Among them, sonochemical synthesis method is advantageous for the synthesis of nanoparticles due to simple, good control of size, highly monodispersed nanoparticles, and very small nanoparticles, etc. **[19-20]**. The sonochemical synthesis technique is one of the most promising chemical synthesis technique for nanoparticles, where the sonochemistry arises from acoustic cavitation phenomenon, i.e., the formation, the growth and the collapse of bubbles in liquid medium **[21]**. In sonochemical synthesis, during ultrasound irradiation, sound waves propagate through the liquid and at the same time microbubbles are created. These microbubbles receive energy and undergo rapid inertial overgrowth until they implode inward catastrophically through a series of stages collectively referred as cavitation **[22]**. Within a microsecond, the cavitation bubble collapse occurs and creates local 'hot spots' with a generation of high local temperature (10,000 K) and pressures (10,000 atm), which fuel the homolysis of water and other present surfactants in the system **[23]**. Besides nanoparticle synthesis, there is a various application of ultrasonic irradiation such as dispersion, extraction, catalysis, adsorption, and production of graphene, etc. **[24]**. A. Asfaram *et. al.* **[25]** reported the ultrasound-assisted simultaneous adsorption of brilliant green (BG) and malachite green (MG) onto Mn-doped Fe_3O_4 nanoparticle-loaded activated carbon (Mn-Fe_3O_4-NP-AC) as a novel adsorbent. Their studies on the well regenerability of the adsorbent in addition to its high adsorption capacity make it promising for such adsorption applications. The enhancement of adsorption capacity with the assistance of ultrasound was due to the hydrodynamic and thermal processes of acoustic cavitation. E. A. Dil *et. al.* **[26]** reported the synthesis of copper oxide nanoparticle-loaded activated carbon (CuO-NP-AC) and used as an efficient adsorbent for the ultrasound-assisted simultaneous removal of the Pb^{2+} ion and malachite green (MG) dye. This research group observed that the combination of ultrasonic power with CuO-NPs-AC is an efficient, fast, low cost and sensitive adsorption process for ultrasound-assisted simultaneous removal of a high content of Pb^{2+} ion and MG dye from aqueous solutions. Further, E. A. Dil *et. al.* **[27-28]** reported the synthesis and characterization of zinc (II) oxide nanorods loaded on activated carbon (ZnO-NRs-AC) to prepare an outstanding adsorbent for the simultaneous adsorption of heavy metals and dyes as hazardous pollutant using ultrasound energy. F. Mehrabi *et al.* **[29]** reported a selective, simple and rapid ultrasound assisted dispersive solid-phase

microextraction (UA-DSPME) developed using cobalt ferrite nanoparticles loaded on activated carbon ($CoFe_2O_4$-NPs-AC) as an efficient sorbent for the preconcentration and determination of Maxilon Red GRL (MR-GRL) dye. H. Gao *et. al.* **[30]** reported a large-scale graphene production by ultrasound-assisted exfoliation of natural graphite in a supercritical CO_2/H_2O medium. This research group's low-cost and time-saving method offers a green and robust access to a large-scale industrial production method for graphene. S. Pradhan *et. al.* **[31]** reported that the effect of different sonication techniques to efficiently prepare particle dispersions from selected non-functionalized nanoparticles (Cu, Al, Mn, ZnO), and corresponding consequences on the particle dose, surface charge, and release of metals. W. Li *et. al.* **[32]** reported the extraction and characterization of natural soil nanoparticles from Chinese soils. This research group used an ultrasonic-centrifugal method to disperse and extract nanoparticles from 12 soils sampled in different regions of China. Recently, M. Abbas *et. al.* **[33-34]** reported the synthesize of monodisperse spinel ferrite nanoparticles using sonochemical and polyol methods. This research group noticed that the sonochemical method could be effectively used for the synthesis of nanocrystalline ferrite with narrow size distribution and also observed the advantages of the sonochemical method over the polyol method in producing highly crystalline, monodisperse nanoparticles with uniform size and shape. M. Abbas *et. al.* **[35]** also reported $CoFe_2O_4$ nanoparticles with uniform shape and size distribution synthesized by a sonochemical method. This research group found that the facile method adopted in their study appears to be a promising route for the synthesis of highly crystalline nanoparticles with in short times and without the need for using any calcination process. M. Sivakumar *et. al.* **[36]** reported a facile route of an ultrasound-assisted synthesis of nanocrystalline manganese zinc ferrite with narrow size distribution. Their simple straightforward sonochemical approach resulted in a better pure phase system of nanoferrite with improved magnetic properties.

A better understanding of structural, magnetic, dielectric, electrical, impedance and modulus spectroscopy characteristics of spinel ferrite nanoparticles is highly beneficial to tune the properties for desired applications. In this work, efforts were carried out to synthesize Gd^{3+} doped cobalt ferrite with chemical formula $CoFe_{2-x}Gd_xO_4$ (x=0.00, 0.05, 0.10, 0.15, 0.20) by a sonochemical method and to investigate their structural, magnetic, dielectric, electrical, impedance and modulus spectroscopy

characteristics. To the best knowledge of authors, this is the first report on Gd^{3+} doped $CoFe_2O_4$ nanoparticles synthesized by a sonochemical method and its physical properties. Interestingly, in the present work, the results demonstrate a significant improvement in dielectric and electrical properties of Gd^{3+} doped cobalt ferrite nanoparticles.

2. Experimental Section

2.1. Synthesis

The series of $CoFe_{2-x}Gd_xO_4$ (x =0.00, 0.05, 0.10, 0.15, 0.20) nanoparticles were prepared by sonochemical method. Analytical grade cobalt nitrate ($Co(NO_3)_2.6H_2O$), iron nitrate ($Fe(NO_3)_3.9H_2O$), gadolinium nitrate ($Gd(NO_3)_3{\cdot}6H_2O$) were chosen as a source material for Co, Fe and Gd, respectively. An aqueous solution of starting precursors (Co, Fe and Gd) in their stoichiometric ratio was prepared by dissolving in deionized water. In this prepared starting precursors solution, an aqueous solution of NaOH was mixed with constant stirring using magnetic stirrer. Further, the mixed solution was exposed to high-intensity ultrasonic irradiation (frequency: 20 kHz and power: 70 W) (Ultrasonic homogenizer UZ SONOPULS HD 2070) for 60 min (Supplementary Material **Fig.S.1**). After 60 min of ultrasonic irradiation, the reaction temperature was 90 ^oC. The prepared nanoparticles were separated by centrifuge process. The obtained nanoparticles were washed several times in deionized water for complete removal of sodium ions. Then, the obtained washed nanoparticles were dried at 60 ^oC for 24 hours.

2.2. Characterization

The crystal structure of synthesized $CoFe_{2-x}Gd_xO_4$ (x=0.0, 0.05, 0.10, 0.15, 0.20) nanoparticles were investigated on Rigaku MiniFlex 600 X-ray Spectrometer with a filtered cobalt source. Raman spectroscopy of prepared spinel ferrite nanoparticles was carried out by using dispersive Raman microscope Nicolet DXR equipped with excitation laser and excitation wavelength 780 nm. The morphology of prepared nanoparticles was studied by using scanning electron microscope Nova NanoSEM450 (FEI company). The Fourier Transform Infrared Spectroscopy of synthesized spinel ferrite nanoparticles were carried out using FTIR spectrometer Nicolet 6700 from Thermo Scientific. The X-ray photoelectron spectroscopy was studied using Kratos Analytical Axis Ultra DLD. The magnetic measurements of synthesized spinel ferrite magnetic nanoparticles were

examined by using a vibrating sample magnetometer (VSM 7407, Lake Shore) at room temperature. Further, the dielectric properties of nanoparticles were investigated using a Broadband Dielectric Impedance Analyzer Concept 40 (Novocontrol, Germany). The sample dimension for dielectric and electrical property measurement was 20 mm in diameter and 0.5 mm in thickness. In addition, the modulus and impedance spectra of prepared spinel ferrite nanoparticles were examined by using a standard sample cell BDS 1200 employing RC model.

3. Result and Discussion

3.1. Structural Study

Fig.1 depicts the X-ray diffraction (XRD) patterns of the $CoFe_{2-x}Gd_xO_4$ (x =0.00, 0.05, 0.10, 0.15, 0.20) nanoparticles synthesized by sonochemical method. All composition of the synthesized $CoFe_{2-x}Gd_xO_4$ (x =0.00, 0.05, 0.10, 0.15, 0.20) nanoparticles could be indexed as a cubic spinel ferrite structure. All the diffraction peaks are well matched with standard $CoFe_2O_4$ (PDF Card No.: 00-002-1045) for X-rays (1.78897 Å for Co Kα) **[37]**. Further, we can notice from **Fig.1**, that there is no evidence of secondary phase such as $GdFeO_3$ in all composition for synthesized $CoFe_{2-x}Gd_xO_4$ (x =0.00, 0.05, 0.10, 0.15, 0.20) nanoparticles. C. Murugesan *et. al.* **[38]** reported that the ionic radius of the Gd^{3+} ion is 0.938 Å, and it is higher than that of the Fe^{3+} ion (0.67 Å). Therefore, a number of Fe^{3+} ions replaced by Gd^{3+} ions are limited and consequently, there is a solubility limit for the replacement of Fe^{3+} ions by Gd^{3+} ions in cobalt ferrite lattice. This research group noticed that excess Gd^{3+} ions tend to aggregate around the grain boundaries in the form of $GdFeO_3$. In this research group work, the optimized maximum solubility limit for the Gd^{3+} ions in cobalt ferrite synthesized by a sol-gel combustion method, was x= 0.10. In our present work, the absence of secondary phase $GdFeO_3$ up to x =0.20 in $CoFe_{2-x}Gd_xO_4$ nanoparticles, indicate ultrasonic irradiation during sonochemical synthesis helps in the formation of single spinel crystal phase Gd^{3+} ion substituted cobalt ferrite nanoparticles in comparison to sol-gel combustion method. In sonochemical synthesis, the ultrasonic irradiation of aqueous medium causes dissociation of water molecules in the cavitation bubbles during transient collapse generating H^* and $^*OH$ radicals **[39]**. Further, few of them may undergo recombination generating H_2 and H_2O_2. The sonochemical hydrolysis of cobalt nitrate, iron nitrate and gadolinium

nitrate generate its hydroxide and further this hydroxide formed its oxide due to H_2O_2 generated by ultrasound cavitation. These formed oxide CoO, Gd_2O_3 and Fe_3O_4 under the influence of ultrasonic wave formed $CoFe_{2-x}Gd_xO_4$ nanoparticles. M. Sivakumar *et. al.* **[40-41]** reported the fabrication of zinc ferrite nanoparticles using ultrasonic irradiation (frequency 20 kHz and power 70 W). This research group also proposed the ultrasonic cavitation mediated formation of $ZnFe_2O_4$ nanoparticles via formation of oxides by sonochemical hydrolysis of precursors.

The average crystallite size of $CoFe_{2-x}Gd_xO_4$ (x =0.00, 0.05, 0.10, 0.15, 0.20) nanoparticles was calculated from the line width of the (311) diffraction peak using Scherrer's equation.

$$D = \frac{0.9\lambda}{\beta\, Cos\theta}$$

where, 'D' is the crystallite size, 'λ' is the wavelength of Co Kα radiation (1.78897 Å), 'β' is the FWHM, 'θ' is the diffraction angle of the strongest characteristic peak. The calculated average crystallite size of sonochemically synthesized $CoFe_{2-x}Gd_xO_4$ nanoparticles are tabulated in **Table 1**, as a function of gadolinium ion concentration in cobalt ferrite nanoparticles. It can be noticed that the crystallite size decreases from 9.2 nm to 7.6 nm when the substitution of Gd^{3+} increases (0.00 – 0.20). The Gd^{3+}-O^{2-} has high bond energy as compared to the Fe^{3+}-O^{2-}, therefore, more energy is required to substitute Gd^{3+} ion at octahedral sites in spinel cobalt ferrite **[42]**. This required energy is obtained at the expense of crystallization and consequently hindrance in the growth of crystallite of spinel ferrite. This provides smaller crystallite sized nanoparticles with an increase of substitution of Gd^{3+} ion in cobalt ferrite nanoparticles.

The lattice constant 'a' was calculated using the following relation:

$$a = d\sqrt{h^2 + k^2 + l^2}$$

where, (h k l) are the Miller indices and 'd' is the inter-planar spacing. The calculated value of lattice constant of sonochemically synthesized $CoFe_{2-x}Gd_xO_4$ nanoparticles is tabulated in **Table 1**. It is noticeable from **Table 1**, that the lattice constant 'a' decreases gradually from 8.3752 Å (x=0.00) to 8.3470 Å (x=0.20) with an increase of gadolinium ion concentration in ferrite nanoparticles. This is due to the larger ionic radius of gadolinium ions in cobalt ferrite, and thereby leads to lattice distortion which results in the lower degree of alignments of lattice fringes. J. Peng *et. al.* **[43]** also observed the

decrease of lattice constant with the increase of gadolinium ion in cobalt ferrite nanoparticles synthesized by hydrothermal method.

The X-ray density (d_x) of the $CoFe_{2-x}Gd_xO_4$ (x =0.00, 0.05, 0.10, 0.15, 0.20) nanoparticles can be calculated as

$$d_x = \frac{8M}{Na^3}$$

where, 'M' is the atomic weight of spinel ferrite sample, 'N' is Avogadro's number (6.022×10^{23} mol^{-1}) and 'a' is the lattice constant. The X-ray density (d_x) of $CoFe_{2-x}Gd_xO_4$ nanoparticles is tabulated in **Table 1**. It can be notice from **Table 1**, that the X-ray density (d_x) increases from 5.305 g/cm^3 (x=0.00) to 5.822 g/cm^3 (x=0.20) with increase of Gd^{3+} ion concentration in cobalt ferrite nanoparticles. The increase in the value of the X-ray density (d_x) is associated with higher molecular weight of spinel cobalt ferrite samples with Gd^{3+} ion.

3.2. Bond length and bond angles

In spinel ferrite, the magnetic property depends on exchange interactions which is also associated with bond length and bond angles between the metal ions. The bond length between cation-anion (p, q, r & s), cation-cation (b, c, d, e & f) and the bond angles (θ_1, θ_2, θ_3, θ_4 and θ_5) between the cations and cation-anion (as shown in Supplementary Material **Fig. S.2)** , are calculated by following relations **[44]**:

Cation-anion distance	Cation-cation distance	Bond angle
$p = a(5/8 - u)$	$b = \sqrt{2}(a/4)$	$\theta_1 = cos^{-1}\left(\frac{p^2 + q^2 - c^2}{2pq}\right)$
$q = a\sqrt{3}(u - 1/4)$	$c = \sqrt{11}\,(a/8)$	$\theta_2 = cos^{-1}\left(\frac{p^2 + r^2 - e^2}{2pr}\right)$
$r = a\sqrt{11}(u - 1/8)$	$d = \sqrt{3}(a/4)$	$\theta_3 = cos^{-1}\left(\frac{2p^2 - b^2}{2p^2}\right)$
$s = a\sqrt{3}\,(u/3 + 1/8)$	$e = \sqrt{3}\,(3a/8)$	$\theta_4 = cos^{-1}\left(\frac{p^2 + s^2 - f^2}{2ps}\right)$

$$f = \sqrt{6}\,(a/4) \qquad \theta_5 = cos^{-1}\left(\frac{r^2 + q^2 - d^2}{2rq}\right)$$

The calculation of bond length between cation-anion (p, q, r & s), cation-cation (b, c, d, e & f) vary in accordance with the variation of lattice constant with Gd^{3+} ion substitution in cobalt ferrite nanoparticles (**Table 2**). Further, the calculation of bond angles, as mentioned in **Table 3**, indicate the decrease in θ_1, θ_2, θ_3, θ_4, and θ_5 with the increase of Gd^{3+} ion substitution in cobalt ferrite nanoparticles. It is well known that the bond angles θ_1, θ_2 and θ_5 are associated with A-B and A-A exchange interactions, whereas θ_3 and θ_4 are related with B-B interaction **[45]**. The decrease in the bond angles θ_1, θ_2 and θ_5 indicate weakening of A-B and A-A interaction. Further, the decrease in the value of the bond angles θ_3 and θ_4 also indicates the weakening of B-B exchange interaction **[46]**.

3.3. Raman Spectroscopy

Raman Spectroscopy is a powerful characterization tool to investigate the structural characteristics of spinel ferrite nanoparticles. **Fig 2** shows the Raman spectra of Gd^{3+} doped cobalt ferrite nanoparticles synthesized by a sonochemical method. The substitution of Gd^{3+} ions in cobalt ferrite nanoparticles rearranges the cations in a unit cell and the ionic size of cations modifies the unit cell parameters such as lattice constant, bond length and bond angles, etc. Consequently, it modifies the Raman modes of Gd^{3+} doped cobalt ferrite nanoparticles **[47]**. A unit cell of a cubic spinel ferrite has eight molecules and the fcc unit cell of spinel ferrite give rise to A_{1g}, $2A_{2u}$, E_g, $2E_u$, F_{1g}, $5F_{1u}$, $3T_{2g}$, and $2F_{2u}$, vibration modes. Here, A, E and T notations correspond to one, two and three dimensional representations, respectively, and 'g' and 'u' denote the symmetric and anti-symmetric modes with respect to the center of inversion. Only five Raman modes, i.e., A_{1g}, E_g, and $3T_{2g}$ are active in spinel ferrite **[48-49]**. The observed Raman bands for Gd^{3+} doped cobalt ferrite nanoparticles are tabulated in **Table 4**. The observed Raman bands at 171-180 cm^{-1}, 284-299 cm^{-1}, 472-479 cm^{-1}, 542-561 cm^{-1}, 624-635 cm^{-1}, 687-689 cm^{-1} were assigned as $T_{2g}(3)$, E_g, $T_{2g}(2)$, $T_{2g}(1)$, $A_{1g}(2)$ and $A_{1g}(1)$, respectively. The high-frequency Raman mode $A_{1g}(1)$ is associated with symmetric stretching mode of vibration at tetrahedral (A) site. Whereas, the sub-band of Raman band $A_{1g}(1)$, i.e., Raman band $A_{1g}(2)$ may be

associated with Co-O bonds at tetrahedral (A) site. This sub-band or splitting of bands indicates the mixed ordering of Co and Fe in synthesized Gd^{3+} doped cobalt ferrite nanoparticles **[50]**. The Raman mode E_g is due to symmetric bending of oxygen ion with respect to iron ion. The $T_{2g}(1)$ is an anti-symmetric bending of oxygen with respect to iron, the $T_{2g}(2)$ mode is the anti-symmetric stretch of iron and oxygen, and the $T_{2g}(3)$ mode is due to the translational motion of Fe-O **[51]**. It is noticeable from **Fig. 2** and **Table 4**, that the frequency of Raman modes was slightly changed with addition of Gd^{3+} ion in cobalt ferrite nanoparticles. This variation in Raman modes with the variation of substitution of Gd^{3+} in cobalt ferrite nanoparticles is associated with redistribution/migration of cations among tetrahedral and octahedral sites **[52]**.

3.4. Fourier Transform Infrared (FTIR) Spectroscopy

FTIR spectra of $CoFe_{2-x}Gd_xO_4$ (x=0.00, 0.05, 0.10, 0.15, 0.20) nanoparticles synthesized by a sonochemical method (Supplementary Material **Fig.S.3**), and the observed absorption band position are tabulated in **Table 1**. Generally, the infrared spectra of spinel ferrite consist of two strong absorption bands, ν_1 (540-600 cm^{-1}) associated with the stretching vibration of the tetrahedral metal oxygen bond and ν_2 (330-400 cm^{-1}) attributed to the octahedral metal oxygen bond **[53]**. The existence of ν_1 and ν_2 absorption bands confirm the formation of spinel ferrite structure of synthesized nanoparticles by sonochemical method. The difference between ν_1 and ν_2 absorption bands is due to the change in bond length (Fe-O) at the tetrahedral and octahedral site **[54]**. Further, the shift in the position of absorption bands with the substitution of Gd^{3+} in cobalt ferrite nanoparticles can be noticed from Supplementary Material **Fig.S.3** and **Table 1**. The variation in absorption band position is due to cation redistribution/migration among tetrahedral and octahedral sites in Gd^{3+} doped cobalt ferrite nanoparticles **[55]**. The force constant of ions at the tetrahedral and octahedral site can be calculated using frequencies ν_1 and ν_2 in the following relation **[56]:**

$$F = 4\pi^2 c^2 \nu^2 \mu,$$

where F is the force constant, c is the light velocity 2.99 x 10^8 m/sec, ν is the vibration frequency of the tetrahedral and octahedral sites, μ is the reduced mass for the Fe^{3+} ions and the O^{2-} ions (~2.065 x 10^{-26} kg/mol). The calculated value of force constant F_T and F_B for tetrahedral and octahedral sites,

respectively, are mentioned in **Table 1**. The variation in force constant indicates variation in bond length of cations and oxygen ion at the tetrahedral and octahedral site in synthesized Gd^{3+} doped spinel cobalt ferrite nanoparticles.

3.5. Morphology and EDX study

The Scanning Electron Microscopy is employed to investigate the morphology of synthesized spinel ferrite nanoparticles. **Fig.3 (a)** shows scanning electron microscopy (SEM) image of $CoFe_{2-x}Gd_xO_4$ (x=0.20) nanoparticles synthesized by sonochemical method. It can be noticed from SEM image that the synthesized spinel ferrite nanoparticles were spherical in morphology with particle size 5- 30 nm. The elemental composition of synthesized Gd^{3+} doped cobalt ferrite nanoparticles was studied by energy dispersive X-ray (EDX) spectrometer attached with SEM. **Fig. 3 (b)** shows the EDX spectrum of $CoFe_{2-x}Gd_xO_4$ (x=0.20) nanoparticles. Typical EDX spectrum reveals the presence of Co, Fe, O and Gd in synthesized spinel ferrite nanoparticles.

3.6. XPS Study

Fig. 4 depicts X-ray photoelectron spectrum of $CoFe_{2-x}Gd_xO_4$ (x = 0.10 & 0.20) nanoparticles synthesized by sonochemical method. To determine the valence state and cation distribution of cobalt and iron at octahedral and tetrahedral sites in synthesized spinel ferrite nanoparticles, Co 2p and Fe 2p high-resolution XPS spectra were studied. In the Co 2p spectra, **Fig. 4 (a)**, there are two main peaks with satellite peak at higher binding energy, these peaks can be assigned as Co $2p_{3/2}$ and Co $2p_{1/2}$ in synthesized spinel ferrite $CoFe_{2-x}Gd_xO_4$ (x= 0.10) nanoparticles. The existence of Co $2p_{3/2}$ peak with satellite peak attributes the existence of Co^{2+} in synthesized nanoparticles **[57]**. Further, in the Fe 2p spectra, **Fig. 4 (b)**, there are two peaks, named as Fe $2p_{3/2}$ and Fe $2p_{1/2}$, with satellite peak at higher binding energy side of these peaks. The presence of Fe $2p_{3/2}$ peak with satellite peak indicate the existence of Fe^{3+} in spinel ferrite $CoFe_{2-x}Gd_xO_4$ (x= 0.10) nanoparticles **[58]**. Similar results were also noticed for synthesized spinel ferrite $CoFe_{2-x}Gd_xO_4$ (x= 0.20) nanoparticles. The asymmetric nature of Co $2p_{3/2}$ and Fe $2p_{3/2}$ peaks indicate the distribution of cation at octahedral and tetrahedral sites in synthesized spinel ferrite nanoparticles. After fitting, the evaluated value of cation distribution Co^{2+}

and Fe^{3+} at tetrahedral and octahedral site in synthesized spinel ferrite $CoFe_{2-x}Gd_xO_4$ (x = 0.10 & 0.20) nanoparticles is tabulated in **Table 5**. These results indicate that synthesized Gd^{3+} doped cobalt ferrite nanoparticles have a composition containing Fe^{3+} and Co^{2+} ions and the presence of Fe and Co at the octahedral and tetrahedral site; and indicate, in addition, cation redistribution with the substitution of Gd^{3+} ions.

3.7. Magnetic Property

Fig. 5 shows the magnetic hysteresis curves for $CoFe_{2-x}Gd_xO_4$ (x=0.00, 0.05, 0.10, 0.15, 0.20) nanoparticles. The magnetic hysteresis curves of synthesized spinel ferrite nanoparticles were obtained by vibrating sample magnetometer at room temperature with an applied magnetic field ±10 kOe. The hysteresis curves demonstrate the variation of magnetic behaviour of Gd^{3+} doped $CoFe_2O_4$ nanoparticles synthesized by a sonochemical method. The magnetic property of spinel ferrite nanoparticles depends on several factors such as substitution of cations, cation redistribution at tetrahedral and octahedral sites, crystallite size, crystallinity, preparation method, etc. **[59]**. The observed value of saturation magnetization (M_s), coercivity (H_c), remanent magnetization (M_r), ratio of remanence to saturation magnetization (M_r/M_s), anisotropy constant (K), magnetic moment (η_B), Yafet-Kittel angle (α_{Y-K}) and initial permeability (μ_i) have been calculated and tabulated in **Table 6**. It can be notice that the value of saturation magnetization (M_s) decreases from 40.19 emu/g to 21.58 emu/g for x = 0.00 - 0.20 in synthesized $CoFe_{2-x}Gd_xO_4$ nanoparticles. The decrease in value of saturation magnetization in $CoFe_{2-x}Gd_xO_4$ nanoparticles is associated with an increase of Gd^{3+} concentrations. The ionic radius of Gd^{3+} ion is larger as compared with Fe^{3+} and Co^{2+}, therefore, it prefers to occupy octahedral (B) sites in spinel cobalt ferrite nanoparticles. Since gadolinium behaves ferromagnetic at just below 16 ^oC, therefore, it is paramagnetic at room temperature (27 ^oC) **[60]**. Hence, substitution of Gd^{3+} ion in cobalt ferrite nanoparticles is equivalent to substitution of non-magnetic ions at octahedral (B) sites in spinel cobalt ferrite lattice. With an increase of concentration of paramagnetic Gd^{3+} ions at octahedral (B) sites in cobalt ferrite nanoparticles, the ferrimagnetic ordering in cobalt ferrite becomes disturbed and A-B superexchange interaction is deteriorated, and consequently, decrease in magnetization of Gd^{3+} doped cobalt ferrite nanoparticles **[61]**. Further, with

the substitution of Gd^{3+} ion in cobalt ferrite, the saturation magnetization decreases with the decrease of crystallite size. This is associated with the surface effect of spinel ferrite magnetic nanoparticles due to small crystallite size **[62]**. This surface effect attributes the existence of a dead magnetic layer associated with the surface spin disorder. The number of spin disorder of Gd^{3+} substituted cobalt ferrite nanoparticles increases with a decrease of crystallite size **[63]**. Moreover, the variation in coercivity (H_c) of Gd^{3+} doped cobalt ferrite nanoparticles is tabulated in **Table 6**. It is noticeable from **Table 6** that the coercivity of $CoFe_{2-x}Gd_xO_4$ nanoparticles initially decreases remarkably from 234.32 Oe (x = 0.00) to 12.60 Oe (x = 0.05) and then increases up to 68.62 Oe (x = 0.20) with increase of Gd^{3+} in cobalt ferrite nanoparticles. The remarkable decrease in coercivity at x = 0.05 in $CoFe_{2-x}Gd_xO_4$ nanoparticles is attributed to the larger lattice distortion and smaller crystallite size **[64]**. Further increase in coercivity with the increase of Gd^{3+} (x=0.10 - 0.20) is associated with the decrease of crystallite size. As coercivity is inversely proportional to grain size and the bigger grains provide less pinning of domain walls due to the lower volume fraction of grain boundaries **[65]**. The coercivity of spinel ferrite nanoparticles depends on several factors such as magneto crystalline anisotropy constant, distortion, cation distribution, porosity, grain size, etc. **[66]**. The anisotropy constant of synthesized spinel ferrite nanoparticles can be calculated by following relation **[67]**:

$$H_c = \frac{0.96\,K}{M_S}$$

where, *K* is anisotropy constant.

The experimental values of magnetic moments per formula unit were calculated from the following relation **[68]**:

$$\eta_B = \frac{M_w M_s}{5585}$$

where, M_w is the molecular weight of the $CoFe_{2-x}Gd_xO_4$ (x = 0.00, 0.05, 0.10, 0.15, 0.20) nanoparticles. The observed value of magnetic moment (η_B) is mentioned in **Table 6**. It is noticeable from **Table 6** that the value of the magnetic moment of Gd^{3+} doped cobalt ferrite decreases with the increase of Gd^{3+} concentration. Yafet-Kittel (Y-K) angle, $\alpha_{y\text{-}k}$, can be evaluated for synthesized spinel ferrite nanoparticles by following relation **[69]**:

$$\eta_B = (6 + x)Cos\alpha_{y-k} - 5\ (1 - x)$$

The evaluated value of Y-K angles for synthesized nanoparticles are tabulated in **Table 6**. It can be noticed from **Table 6**, that the Y-K angle increases with the increase of Gd^{3+} substitution in cobalt ferrite nanoparticles, which indicate the presence of triangular spin arrangement of ions **[70]**. The initial permeability (μ_i) can be calculated from the following relation **[71]**:

$$\mu_i = M_S^2 * \frac{D}{K}$$

where, M_s is saturation magnetization, D is the grain size, and K is magnetocrystalline anisotropy. The calculated value of initial permeability is tabulated in **Table 6**. The initial permeability was increased initially remarkably from 1.514 (x=0.00) to 26.321 (x=0.05) in $CoFe_{2-x}Gd_xO_4$ nanoparticles, and then further decreased to 2.298 (x=0.20) with increase of Gd^{3+} concentration and decrease of grain size. It represents the dependence on magnetocrystalline anisotropy unpaired electrons and coercivity on the initial permeability **[72]**.

3.8. Dielectric Property

3.8.1. Real and Imaginary Part of Dielectric

Fig.6 depicts frequency dependence real and imaginary part of dielectric constant (ε' and ε'') for $CoFe_{2-x}Gd_xO_4$ (x = 0.00, 0.05, 0.10, 0.15, 0.20) nanoparticles. It is noticeable from **Fig.6** that the dielectric constant decreases with the increase of frequency. At low-frequency region, the dielectric constant decreases sharply, whereas, at high-frequency region, it becomes frequency independent. It can be explained with the knowledge of the structure of spinel ferrite and Koop's model **[73]**. In view of Koop's model, spinel ferrite is composed of remarkably conducting layers known as grains, accompanied by poorly conducting layers known as grain boundaries **[74]**. At low frequency, the grain boundaries are more effective than grain, thereby, the dielectric constant is high at low frequency and it decreases with the increase of frequency **[75]**. In the influence of applied ac electric field, as electrons reach on the poorly conducting grain boundaries, these electrons pile up there and it creates space charge polarization. Because of this, the dielectric constant is high at low frequency, and a further increase of frequency, decreases the dielectric constant. The decrease in dielectric constant

occurs when the charge carries cannot follow the applied ac electric field beyond a certain critical frequency. Further, in view of Rabinkin and Novikova **[76],** the polarization in spinel ferrite is through electron exchange between Fe^{2+} and Fe^{3+}. The local displacement of these electrons in the direction of applied ac electric field determine the polarization. With an increase of frequency, this polarization decreases and attains a constant value because, beyond a certain frequency of applied ac electric field, the electron exchange between Fe^{2+} and Fe^{3+} cannot follow the applied ac electric field **[77]**. As the particle size decreases to nano-regime, the volume fraction of the particle increases, and hence space polarization plays a major role on the dielectric constant of the material. It can be noticed from **Fig. 6** that the dielectric constant increases with an increase of Gd^{3+} in cobalt ferrite nanoparticles. With an increase of Gd^{3+} in cobalt ferrite, or in another view, with a decrease of grain size of this ferrite nanoparticles, the surface effect increases and hence the grain boundaries are more effective at the lower frequency in smaller grain size spinel ferrite nanoparticles, this results in the increase in the value of dielectric constant. In another way, the substitution of Gd^{3+} in cobalt ferrite nanoparticles results in the migration the Co^{2+} ions to tetrahedral sites, as noticed in XPS study, creates the strain in the lattice and to relieve this strain, an equal amount of Fe^{3+} ions can migrate from the tetrahedral site to octahedral site. It increases the hopping of electron between Fe^{2+} and Fe^{3+} at octahedral sites in spinel ferrite and consequently increases in the value of dielectric constant with an increase of Gd^{3+} substitution in cobalt ferrite nanoparticles (**Table 7**).

3.8.2. Dielectric loss (tan δ)

The frequency dependence dielectric loss (tan δ) of $CoFe_{2-x}Gd_xO_4$ (x=0.00, 0.05, 0.10, 0.15, 0.20) nanoparticles is shown in Supplementary Material **Fig.S.4** and observed value is tabulated in **Table 7**. It can be noticed that the dielectric loss decreases with an increase of frequency at low frequency, whereas, it becomes frequency independent at the higher frequency. At low frequency, the high value of the dielectric loss is associated with high resistivity (i.e., poor conductivity) of grain boundaries which are more dominant at low frequency **[78]**. Because of high resistivity of grain boundaries more energy is required for electron exchange between Fe^{2+} and Fe^{3+} and consequently more energy loss **[79]**. Further, with an increase in frequency, less energy is required to electron exchange, and thereby

less dielectric loss. Furthermore, when the frequency of applied ac electric field is equal to the hopping frequency of the charge carriers, the maximum energy is transferred to the oscillating ions and consequently appearance of dielectric loss peak **[80]**.

3.9. AC Conductivity

The conductivity of material relates the macroscopic measurement to the microscopic movement of the charge carriers. The frequency dependence ac conductivity of $CoFe_{2-x}Gd_xO_4$ (x=0.00, 0.05, 0.10, 0.15, 0.20) nanoparticles is shown in Supplementary Material **Fig.S.5**. It can be noticed that the electrical conductivity of synthesized spinel ferrite nanoparticles increases slowly at low frequency, whereas, it increases rapidly at a higher frequency. The electrical conductivity in spinel ferrite material is due to hopping of electrons between the same element present in more than one valence state. The existence of Fe and Co ions at octahedral sites in synthesized spinel ferrite nanoparticles may cause conduction according to following relation **[81]**:

$Co^{2+} + Fe^{3+} \leftrightarrow Co^{3+} + Fe^{2+}$

The electron can migrate in between Fe^{2+} and Fe^{3+} present at the octahedral site in spinel ferrite nanoparticles under the influence of applied ac electric field and its contribute to the electrical response of synthesized nanoparticles. Further, an increase in Fe^{3+} ions at the octahedral sites with the substitution of Gd^{3+} in cobalt ferrite nanoparticles, plays an important role in enhancing the ac conductivity of $CoFe_{2-x}Gd_xO_4$ nanoparticles (**Table 7**) **[38]**.

3.10. Impedance and Modulus Spectroscopy

Fig. 7 depicts the variation of real part of impedance (Z') and modulus (M') of $CoFe_{2-x}Gd_xO_4$ (x = 0.00, 0.05, 0.10, 0.15, 0.20) nanoparticles synthesized by sonochemical method. It can be noticed from **Fig. 7** that the Z' decreases with an increase of frequency. It correlates the increase of electrical conductivity of synthesized spinel ferrite nanoparticles with an increase of the frequency. At high frequency, the value of Z' coincided for ferrite nanoparticles which indicate the possible release of space charge. It can be also noticed from **Fig. 7** that the value of Z' decreases with an increase of substitution of Gd^{3+} in cobalt ferrite nanoparticles, which support the observed the increase in

conductivity with an increase of Gd^{3+} in ferrite nanoparticles. Further, at low frequency, the value of real part of the modulus (M') tend to a very small value, i.e., approaching to zero, indicate negligible contribution of electrode effect **[82]**. With an increase of frequency, a continuous dispersion of M' is due to conduction mechanism related to mobility of charge carriers **[83]**.

Fig. 8 depicts the variation of imaginary part of impedance (Z'') and modulus (M'') of $CoFe_{2-x}Gd_xO_4$ (x=0.00, 0.05, 0.10, 0.15, 0.20) nanoparticles synthesized by sonochemical method. It can be noticed from **Fig.8** that sample at x = 0.00, the M'' spectrum has two M'' peaks which is associated with the contribution of grain boundary and grain, whereas at higher concentration, M'' has a single peak. The higher frequency side of the M'' peak, indicates the range of frequencies in which the ions are spatially confined to their potential wells, whereas, the low-frequency side of the M'' peak, indicates the range of frequency in which charge carriers are mobile over long distances **[84]**. **Fig. 9** shows the Cole-Cole plot for $CoFe_{2-x}Gd_xO_4$ (x=0.00, 0.05, 0.10, 0.15, 0.20) nanoparticles synthesized by sonochemical method. The cobalt ferrite nanoparticles (at x =0.00) exhibit two successive semicircles, first semicircles at low frequency, represents the contribution of grain boundary, and the second one at high frequency, reveals the contribution of grain to conduction mechanism. With the substitution of Gd^{3+} in cobalt ferrite nanoparticles, the second semicircles related to the contribution of grain was diminished. The existence of one semicircle at higher concentration of Gd^{3+} in cobalt ferrite nanoparticles, indicate the grain boundary effect is dominant one in the conduction mechanism. The parameters τ_{gb}, C_{gb}, and R_{gb} correspond to the relaxation time, capacitance and resistance for the grain boundary, were calculated using the following relations **[85-87]**:

$$\tau = \frac{1}{2\pi f_{M''}}$$

$$M'' = \frac{\varepsilon_o}{2C}$$

$$2\pi fRC = 1$$

The calculated parameters τ_{gb}, C_{gb}, and R_{gb} were tabulated in **Table 7.** The calculated values of grain boundary relaxation time (τ_{gb}) for synthesized spinel ferrite nanoparticles were within the range of 0.9 μs - 36.0 μs. The calculated values of grain boundary capacitance (C_{gb}) were within the range of 63.3 pF – 82.0 pF. Further, the grain boundary resistance (R_{gb}) were within the range of 14.5 KΩ - 513

KΩ. These parameters were varied with the variation of microstructure and grain size with the substitution of Gd^{3+} in cobalt ferrite nanoparticles.

4. Conclusion

In this present work, a facile and green method for Gd^{3+} doped cobalt ferrite nanoparticles of a single spinel crystal phase with chemical formula $CoFe_{2-x}Gd_xO_4$ (x= 0.00, 0.05, 0.10, 0.15, 0.20) under ultrasonic irradiation was reported. The influence of Gd^{3+} ion in cobalt ferrite nanoparticles on structural, magnetic, dielectric, electrical, impedance and modulus spectroscopic characteristics were investigated. X-ray diffraction study confirmed that sonochemical synthesis is favourable to form single spinel crystal phase gadolinium ions doped cobalt ferrite nanoparticles with higher concentrations of gadolinium, up to x=0.20. The average crystallite size decreases with the substitution of Gd^{3+} in cobalt ferrite nanoparticles. Raman and Fourier Transform Infrared spectroscopy depicted the influence of Gd^{3+} substitution in cobalt ferrite nanoparticles synthesized by a sonochemical method. X-ray photoelectron spectroscopy demonstrated the influence of Gd^{3+} addition in cobalt ferrite nanoparticles on cation distribution at the tetrahedral and octahedral site. The electrical properties showed that the Gd^{3+} doped cobalt ferrite ($CoFe_{2-x}Gd_xO_4$; x= 0.20) exhibit enhanced dielectric constant (277 at 100 Hz) and ac conductivity (20.2 x 10^{-9} S/cm at 100 Hz). The modulus spectroscopy demonstrated the influence of Gd^{3+} in $CoFe_2O_4$ nanoparticles on the variation of relaxation time, capacitance, and resistance in terms of the grain boundary. Vibrating sample magnetometer measurement revealed that the coercivity decreases with Gd^{3+} substitution in cobalt ferrite nanoparticles from 234.32 Oe (x=0.00) to 12.60 Oe (x=0.05) and further increases from 12.60 Oe (x=0.05) to 68.62 Oe (x=0.20). In addition, saturation magnetization decreases with Gd^{3+} substitution from 40.19 emu/g (x=0.00) to 21.58 emu/g (x=0.20). The obtained results demonstrate that the crystallite size, cation distribution, magnetic, dielectric and electrical properties can be tuned with ultrasonic irradiation and gadolinium substitution in cobalt ferrite nanoparticles of single spinel crystal phase synthesized by a sonochemical method. To the best of our knowledge, this is first report on Gd^{3+} doped $CoFe_2O_4$ nanoparticles synthesized by sonochemical method and its structural, magnetic, dielectric, electrical, modulus and impedance characteristics. The sonochemically

synthesized spinel ferrite nanoparticles can have potential application for magnetic recording and microwave devices. The sonochemical method can be considered to synthesize rare-earth ion doped spinel ferrite nanoparticles to large scale production for industrial application as this method has economic and environmental advantages.

Acknowledgement

This work was supported by the Ministry of Education, Youth and Sports of the Czech Republic – Program NPU I (LO1504).

References

[1]. S. Kamali, Spin structure, magnetism, and cation distributions of $NiFe_{2-x}Al_xO_4$ solid Solutions, Journal of Magnetism and Magnetic Materials 433 (2017) 155–161.

[2]. R. Zhang, Q. Yuan, R. Ma, X. Liu, C. Gao, M. Liu, C.-L. Jia and H. Wang, Tuning conductivity and magnetism of $CuFe_2O_4$ via cation redistribution, RSC Adv. 7 (2017) 21926.

[3]. Y.-W. Jun, J.-W. Seo, J. Cheon, Nanoscaling Laws of Magnetic Nanoparticles and Their Applicabilities in Biomedical Sciences, Accounts of Chemical Research 41 (2008) 179-189.

[4]. A. Kovalenko, R. S. Yadav, J. Pospisil, O. Zmeskal, D. Karashanova, P. Heinrichova , M. Vala, J. Havlica, M. Weiter, Towards improved efficiency of bulk-heterojunction solar cells using various spinel ferrite magnetic nanoparticles, Organic Electronics 39 (2016) 118-126.

[5]. P. N. Anantharamaiah and P. A. Joy, Tuning of the magnetostrictive properties of cobalt ferrite by forced distribution of substituted divalent metal ions at different crystallographic sites, Journal of Applied Physics 121 (2017) 093904.

[6]. X. Lasheras, M. Insausti, I. Gil de Muro, E. Garaio, F. Plazaola, M. Moros, L. De Matteis, J. M. de la Fuente, and L. Lezama, Chemical Synthesis and Magnetic Properties of Monodisperse Nickel Ferrite Nanoparticles for Biomedical Applications, J. Phys. Chem. C 120 (6) (2016) 3492–3500.

[7]. C. Singh, A. Goyal and S. Singhal, Nickel-doped cobalt ferrite nanoparticles: efficient catalysts for the reduction of nitroaromatic compounds and photo-oxidative degradation of toxic dyes, Nanoscale 6 (2014) 7959.

[8]. C. Feng, X. Liu, S. Wing Or, and S. L. Ho, Exchange coupling and microwave absorption in core/shell-structured hard/soft ferrite-based $CoFe_2O_4/NiFe_2O_4$ nanocapsules, AIP Advances 7 (2017) 056403.

[9]. H. L. Andersen and M. Christensen, In situ powder X-ray diffraction study of magnetic $CoFe_2O_4$ nanocrystallite synthesis, Nanoscale 7 (2015) 3481.

[10]. L. T. Lu, N. T. Dung, L. D. Tung, C. T. Thanh, O. K. Quy, N. V. Chuc, S. Maenosono and N. T. K. Thanh, Synthesis of magnetic cobalt ferrite nanoparticles with controlled morphology, monodispersity and composition: the influence of solvent, surfactant, reductant and synthetic conditions, Nanoscale 7 (2015) 19596.

[11]. S. K. Gore, S. S. Jadhav, V. V. Jadhav, S. M. Patange, Mu. Naushad, R. S. Mane & K. H. Kim, The structural and magnetic properties of dual phase cobalt ferrite, Scientific Reports 7, Article number: 2524 (2017).

[12]. R. S. Yadav, J. Havlica, M. Hnatko, P. Šajgalík, C. Alexander, M. Palou, E. Bartoníčková, M. Boháč, F. Frajkorová, J. Masilko, M. Zmrzlý, L. Kalina, M. Hajdúchová, V. Enev, Magnetic properties of $Co_{1-x}Zn_xFe_2O_4$ spinel ferrite nanoparticles synthesized by starch-assisted sol–gel autocombustion method and its ball milling, Journal of Magnetism and Magnetic Materials 378 (2015) 190–199.

[13]. R S Yadav, J Havlica, J Masilko, L Kalina, M Hajdúchová, V Enev, J Wasserbauer, I Kuřitka, Z Kožáková, Structural, Cation Distribution, and Magnetic Properties of $CoFe_2O_4$ Spinel Ferrite Nanoparticles Synthesized Using a Starch-Assisted Sol-Gel Auto-Combustion Method, J. Supercond. Nov. Magn. 28 (2015)1851-1868.

[14]. R. Indhrajothi, I. Prakash, M. Venkateswarlu and N. Satyanarayana, Lanthanum ion (La^{3+}) substituted $CoFe_2O_4$ anode material for lithium ion battery applications, New J. Chem. 39 (2015) 4601-4610.

[15]. K. Kamala Bharathi, R. J. Tackett, C. E. Botez, and C. V. Ramana, Coexistence of spin glass behavior and long-range ferromagnetic ordering in La- and Dy-doped Co ferrite, J. Appl. Phys. 109 (2011) 07A510.

[16]. P. Guo, L. Cui, Y. Wang, M. Lv, B. Wang, and X. S. Zhao, Facile Synthesis of $ZnFe_2O_4$ Nanoparticles with Tunable Magnetic and Sensing Properties, Langmuir 29 (2013) 8997−9003.

[17]. A. Shahul Hameed, H. Bahiraei, M. V. Reddy, M. Z. Shoushtari, J. J. Vittal, C. K. Ong, and B. V. R. Chowdari, Lithium Storage Properties of Pristine and (Mg, Cu) Codoped $ZnFe_2O_4$ Nanoparticles, ACS Appl. Mater. Interfaces 6 (2014) 10744−10753.

[18]. G. Fan, J. Tong, and F. Li, Visible-Light-Induced Photocatalyst Based on Cobalt-Doped Zinc Ferrite Nanocrystals, Ind. Eng. Chem. Res. 51 (2012) 13639−13647.

[19]. R. S. Yadav, P. Mishra, A. C. Pandey, Growth mechanism and optical property of ZnO nanoparticles synthesized by sonochemical method, Ultrasonics Sonochemistry 15 (2008) 863-868.

[20]. P. Mishra, R. S. Yadav, A. C. Pandey, Growth mechanism and photoluminescence property of flower-like ZnO nanostructures synthesized by starch-assisted sonochemical method, Ultrasonics Sonochemistry 17 (2010) 560-565.

[21]. K.S. Suslick, Sonochemistry, Science 247 (1990) 1439–1445.

[22]. K. Muthoosamy, S. Manickam, State of the art and recent advances in the ultrasound-assisted synthesis, exfoliation and functionalization of graphene derivatives, Ultrasonic Sonochemistry 39 (2017) 478-493.

[23]. K. S. Suslick, G. J. Price, Applications of ultrasound to materials chemistry, Annual Review of Materials Science 29 (1999) 295-326.

[24]. J. H. Bang, K. S. Suslick, Applications of Ultrasound to the Synthesis of Nanostructured Materials, Adv. Mater. 22 (2010) 1039–1059.

[25]. A. Asfaram, M. Ghaedi, S. Hajati, A. Goudarzi, E. A. Dil, Screening and optimization of highly effective ultrasound-assisted simultaneous adsorption of cationic dyes onto Mn-doped Fe_3O_4-nanoparticle-loaded activated carbon, Ultrasonics Sonochemistry 34 (2017) 1–12.

[26]. E. A. Dil, M. Ghaedi, A. Asfaram, S. Hajati, F. Mehrabi, A. Goudarzi, Preparation of nanomaterials for the ultrasound-enhanced removal of Pb^{2+} ions and malachite green dye: Chemometric optimization and modelling, Ultrasonics Sonochemistry 34 (2017) 677–691.

[27]. E. A. Dil, M. Ghaedi, A. Asfaram, The performance of nanorods material as adsorbent for removal of azo dyes and heavy metal ions: Application of ultrasound wave, optimization and modelling, Ultrasonics Sonochemistry 34 (2017) 792–802.

[28]. E. A. Dil, M. Ghaedi, A.M. Ghaedi, A. Asfaram, A. Goudarzi, S. Hajati, M. Soylak, S. Agarwal, V. K. Gupta, Modeling of quaternary dyes adsorption onto ZnO–NR–AC artificial neural network: Analysis by derivative spectrophotometry, Journal of Industrial and Engineering Chemistry 34 (2016) 186–197.

[29]. F. Mehrabi, A. Vafaei, M. Ghaedi, A. M. Ghaedi, E. A. Dil, A. Asfaram, Ultrasound assisted extraction of Maxilon Red GRL dye from water samples using cobalt ferrite nanoparticles loaded on activated carbon as sorbent: Optimization and modelling, Ultrasonics Sonochemistry 38 (2017) 672–680.

[30]. H. Gao, K. Zhu, G. Hu, C. Xue, Large-scale graphene production by ultrasound-assisted exfoliation of natural graphite in supercritical CO_2/H_2O medium, Chemical Engineering Journal 308 (2017) 872–879.

[31]. S. Pradhan, J. Hedberg, E. Blomberg, S. Wold, I. O. Wallinder, Effect of sonication on particle dispersion, administered dose and metal release of non-functionalized, non-inert metal nanoparticles, J Nanopart Res 18 (2016) 285.

[32]. W. Li, Y. He,J. Wu, J. Xu, Extraction and characterization of natural soilnanoparticles from Chinese soils, European Journal of Soil Science 63 (2012)754–761.

[33]. M. Abbas, B. Parvatheeswara Rao, C. Gi Kim, Shape and size-controlled synthesis of Ni Zn ferrite nanoparticles by two different routes, Materials Chemistry and Physics 147 (2014) 443-451.

[34]. M. Abbas, S. R. Torati, B. Parvatheeswara Rao, M.O. Abdel-Hamed, C. Gi Kim, Size controlled sonochemical synthesis of highly crystalline superparamagnetic Mn–Zn ferrite nanoparticles in aqueous medium, Journal of Alloys and Compounds 644 (2015) 774–782.

[35]. M. Abbas, B. Parvatheeswara Rao, Md. NazrulIslam, K. Woo Kim, S. M. Naga, M. Takahashi, C. Gi Kima, Size-controlled high magnetization $CoFe_2O_4$ nanospheres and nanocubes using rapid one-pot sonochemical technique, Ceramics International 40 (2014) 3269–3276.

[36]. M. Sivakumar, A. Towata, K. Yasui, T. Tuziuti, T. Kozuka, Y. Iida, M. M. Maiorov, E. Blums, D. Bhattacharya, N. Sivakumar, M. Ashok, Ultrasonic cavitation induced water in vegetable oil emulsion droplets – A simple and easy technique to synthesize manganese zinc ferrite nanocrystals with improved magnetization, Ultrasonics Sonochemistry 19 (2012) 652–658.

[37]. B. Wang, G. Wang, Z. Lv, H. Wang, In situ synthesis of hierarchical $CoFe_2O_4$ nanoclusters/ graphene aerogels and their high performance for lithium-ion batteries, Phys. Chem. Chem. Phys. 17 (2015) 27109 -27117.

[38]. C. Murugesan and G. Chandrasekaran, Impact of Gd^{3+} substitution on the structural, magnetic and electrical properties of cobalt ferrite nanoparticles, RSC Adv. 5 (2015) 73714.

[39]. B. R. Reddy, T. Sivasankar, M. Sivakumar, V. S. Moholkar, Physical facets of ultrasonic cavitational synthesis of zinc ferrite particles, Ultrasonics Sonochemistry 17 (2010) 416–426.

[40]. M. Sivakumar, T. Takami, H. Ikuta, A. Towata, K. Yasui, T. Tuziuti, T. Kozuka, D. Bhattacharya, and Y. Iida, Fabrication of Zinc Ferrite Nanocrystals by Sonochemical Emulsification and Evaporation: Observation of Magnetization and Its Relaxation at Low Temperature, J. Phys. Chem. B 110 (2006) 15234-15243.

[41]. M. Sivakumar, A. Towata, K. Yasui, T. Tuziuti, Y. Iida, A new ultrasonic cavitation approach for the synthesis of zinc ferrite nanocrystals, Current Applied Physics 6 (2006) 591–593.

[42]. J. A. Dean, Lange's handbook of chemistry, McGraw-Hill, New York, 15th edn, 1998.

[43]. J. Peng, M. Hojamberdiev, Y. Xu, B. Cao, J. Wang, H. Wu, Hydrothermal synthesis and magnetic properties of gadolinium-doped $CoFe_2O_4$ nanoparticles, Journal of Magnetism and Magnetic Materials 323 (2011) 133–138.

[44]. P. Thakur, R. Sharma, V. Sharma, P.B. Barman, M. Kumar, D. Barman, S.C. Katyal, P. Sharma, Gd^{3+} doped Mn-Zn soft ferrite nanoparticles: Superparamagnetism and its correlation with other physical properties, Journal of Magnetism and Magnetic Materials 432 (2017) 208-217.

[45]. R. Sharma, P. Thakur, P. Sharma, V. Sharma, Ferrimagnetic Ni^{2+} doped Mg-Zn spinel ferrite nanoparticles for high density information storage, Journal of Alloys and Compounds 704 (2017) 7-17.

[46]. P. P. Naik, R.B. Tangsali, S.S. Meena, S.M. Yusuf, Influence of rare earth (Nd^{3+}) doping on structural and magnetic properties of nanocrystalline manganese-zinc ferrite, Materials Chemistry and Physics 191 (2017) 215-224.

[47]. S. Thota, S. C. Kashyap, S. K. Sharma, V. R. Reddy, Micro Raman, Mossbauer and magnetic studies of manganese substituted zinc ferrite nanoparticles: Role of Mn, Journal of Physics and Chemistry of Solids 91 (2016) 136–144.

[48]. S. Thota, S. C. Kashyap, S. K. Sharma, V.R. Reddy, Cation distribution in Ni-substituted $Mn_{0.5}Zn_{0.5}Fe_2O_4$ nanoparticles: A Raman, Mössbauer, X-ray diffraction and electron spectroscopy study, Materials Science and Engineering B 206 (2016) 69–78.

[49]. K. Sabri, A. Rais, K. Taibi, M. Moreau, B. Ouddane, A. Addou, Structural Rietveld refinement and vibrational study of $MgCr_xFe_{2-x}O_4$ spinel ferrites, Physica B 501 (2016) 38 – 44.

[50]. R. N. Bhowmik, A. K. Sinha, Improvement of room temperature electric polarization and ferrimagnetic properties of $Co_{1.25}Fe_{1.75}O_4$ ferrite by heat treatment, Journal of Magnetism and Magnetic Materials 421 (2017) 120–131.

[51]. A. V. Humbe, A. C. Nawle, A.B. Shinde, K.M. Jadhav, Impact of Jahn Teller ion on magnetic and semiconducting behaviour of Ni-Zn spinel ferrite synthesized by nitrate-citrate route, Journal of Alloys and Compounds 691 (2017) 343-354.

[52]. R. A. Pawar, S. M. Patange, Q. Y. Tamboli, V. Ramanathan, S. E. Shirsath, Spectroscopic, elastic and dielectric properties of Ho^{3+} substituted Co-Zn ferrites synthesized by sol-gel method, Ceramics International 42 (2016) 16096 – 16102.

[53]. P. Samoila, C. Cojocaru, L. Sacarescu, P. P. Dorneanu, A.-A. Domocos, Aurelian Rotaruca, Remarkable catalytic properties of rare-earth doped nickel ferritessynthesized by sol-gel auto-combustion with maleic acid as fuel for CWPO of dyes, Applied Catalysis B: Environmental 202 (2017) 21–32.

[54]. K. Rajasekhar Babu, K. Rama Rao, B. Rajesh Babu, Cu^{2+}-modified physical properties of Cobalt-Nickel ferrite, Journal of Magnetism and Magnetic Materials 434 (2017) 118–125.

[55]. S. Torkian, A. Ghasemi, R. Shoja Razavi, Cation distribution and magnetic analysis of wideband microwave absorptive $Co_xNi_{1-x}Fe_2O_4$ ferrites, Ceramics International 43 (2017) 6987–6995.

[56]. R. S. Yadav, J. Havlica, J. Masilko, L. Kalina, J. Wasserbauer, M. Hajdúchová, V. Enev, I. Kuřitka, Z. Kožáková, Effects of annealing temperature variation on the evolution of structural and magnetic properties of $NiFe_2O_4$ nanoparticles synthesized by starch-assisted sol–gel auto-combustion method, Journal of Magnetism and Magnetic Materials 394 (2015) 439–447.

[57]. Z. Zhou, Y. Zhang, Z. Wang, W. Wei, W. Tang, J. Shi, R. Xiong, Electronic structure studies of the spinel $CoFe_2O_4$ by X-ray photoelectron spectroscopy, Applied Surface Science 254 (2008) 6972-6975.

[58]. T. Magno de Lima Alves, B. Ferreira Amorim, M. Antonio Morales Torres, C. Gomes Bezerra, Suzana N´obrega de Medeiros, P. Lana Gastelois, L. Eugenio Fernandez Outon and W. Augusto de Almeida Macedo, Wasp-waisted behavior in magnetic hysteresis curves of $CoFe_2O_4$ nanopowder at a low temperature: experimental evidence and theoretical approach, RSC Adv. 7 (2017) 22187.

[59]. M.A. Dar, Dinesh Varshney, Effect of d-block element Co^{2+} substitution on structural, Mössbauer and dielectric properties of spinel copper ferrites, Journal of Magnetism and Magnetic Materials 436 (2017) 101–112.

[60]. R. Islam, M.A. Hakim, M.O. Rahman, H. Narayan Das, M.A. Mamun, Study of the structural, magnetic and electrical properties of Gd-substituted Mn–Zn mixed ferrites, Journal of Alloys and Compounds 559 (2013) 174–180.

[61]. S. Joshi, M. Kumar, S. Chhoker, A. Kumar, M. Singh, Effect of Gd^{3+} substitution on structural, magnetic, dielectric and optical properties of nanocrystalline $CoFe_2O_4$, Journal of Magnetism and Magnetic Materials 426 (2017) 252–263.

[62]. M. Vadivela, R. Ramesh Babu, K. Ramamurthi, M. Arivanandhan, Enhanced dielectric and magnetic properties of polystyrene added $CoFe_2O_4$ magnetic nanoparticles, Journal of Physics and Chemistry of Solids 102 (2017) 1–11.

[63]. L. Sun, R. Zhang, Z. Wang, L. Ju, E. Cao, Y. Zhang, Structural, dielectric and magnetic properties of $NiFe_2O_4$ prepared via sol–gel auto-combustion method, Journal of Magnetism and Magnetic Materials 421(2017) 65–70.

[64]. A. K. Nikumbh, R. A. Pawar, D. V. Nighot, G. S. Gugale, M. D. Sangale, M. B. Khanvilkar, A. V. Nagawade, Structural,electrical,magnetic and dielectric properties of rare-earth substituted cobalt

ferrites nanoparticles synthesized by the co-precipitation method, Journal of Magnetism and Magnetic Materials 355 (2014) 201–209.

[65]. R. S. Yadav, J. Havlica, I. Kuritka, Z. Kozakova, M. Palou, E. Bartonıckova, M. Bohac, F. Frajkorova, J. Masilko, L. Kalina, M. Hajduchova, V. Enev, J. Wasserbauer, Magnetic Properties of Dysprosium-Doped Cobalt Ferrite Nanoparticles Synthesized by Starch-Assisted Sol-Gel Auto-combustion Method, J Supercond Nov Magn 28 (2015) 2097–2107.

[66]. D. Pal, M. Mandal, A. Chaudhuri, B. Das, D. Sarkar, and K. Mandal, Micelles induced high coercivity in single domain cobalt-ferrite nanoparticles, J. Appl. Phys. 108 (2010) 124317.

[67]. R. C. Kambale, K. M. Song, Y. S. Koo, and N. Hur, Low temperature synthesis of nanocrystalline Dy^{3+} doped cobalt ferrite: Structural and magnetic properties, J. Appl. Phys. 110 (2011) 053910.

[68]. J. Jadhav, S. Biswas, A.K. Yadav, S.N. Jha, D. Bhattacharyya, Structural and magnetic properties of nanocrystalline NieZn ferrites: In the context of cationic distribution, Journal of Alloys and Compounds 696 (2017) 28-41.

[69]. Ch.S.L.N. Sridhar, Ch.S.Lakshmi, G.Govindraj, S.Bangarraju, LSatyanarayana, D.M. Potukuchi, Structural, morphological, magnetic and dielectric characterization of nano-phased antimony doped manganese zinc ferrites, Journal of Physics and Chemistry of Solids 92 (2016) 70–84.

[70]. M. Tahir Farid, I. Ahmad, M. Kanwal, G. Murtaza, I. Ali, M. Naeem Ashiq, S. Ahmad Khan, Magnetic and electric behaviour of praseodymium substituted $CuPr_yFe_{2-y}O_4$ ferrites, Journal of Magnetism and Magnetic Materials 422 (2017) 337–343.

[71]. M. Niaz Akhtar, A. Rahman, A.B. Sulong, M. Azhar Khan, Structural, spectral, dielectric and magnetic properties of $Ni_{0.5}Mg_xZn_{0.5-x}Fe_2O_4$ nanosized ferrites for microwave absorption and high frequency applications, Ceramics International 43 (2017) 4357–4365.

[72]. S. B. Singh, C.Srinivas, B.V.Tirupanyam, C.L.Prajapat, M.R.Singh, S.S.Meena, P. Bhatt, S.M.Yusuf, D.L.Sastry, Structural, thermal and magnetic studies of $Mg_xZn_{1-x}Fe_2O_4$ nanoferrites: Study of Exchange Interactions on Magnetic Anisotropy, Ceram. Int. 42 (2016) 19179-19186.

[73]. C. G. Koops, On the Dispersion of Resistivity and Dielectric Constant of Some Semiconductors at Audiofrequencies, Phys. Rev. 83 (1951) 121.

[74]. J C Maxwell (1954) A Treatise on Electricity and Magnetism (New York: Oxford University Press).

[75]. R C Kambale, P A Shaikh, C H Bhosale, K Y Rajpure and Y D Kolekar, Dielectric properties and complex impedance spectroscopy studies of mixed Ni–Co ferrites, Smart Mater. Struct. 18 (2009) 085014.

[76]. I T Rabinkin and Z I Novikova (1960) Ferrites Izv Acad. Nauk USSR Minsk 146.

[77]. R G Kharabe, R S Devan, C M Kanamadi and B K Chougule, Dielectric properties of mixed Li–Ni–Cd ferrites, Smart Mater. Struct. 15 (2006) N36–N39.

[78]. R G Kharabe, R S Devan, C M Kanamadi and B K Chougule, Dielectric properties of mixed Li–Ni–Cd ferrites, Smart Mater. Struct. 15 (2006) N36–N39.

[79]. J. Parashar, V. K. Saxena, J. Sharma, D. Bhatnagar, K. B. Sharma, Dielectric Behaviour of $Ni_{0.2}Cu_{0.2}Zn_{0.6}Fe_2O_4$ Spinel Ferrite, Macromol. Symp. 357 (2015) 43–46.

[80]. N. Kumari, V. Kumar and S. K. Singh, Structural, dielectric and magnetic investigations on Al^{3+} substituted Zn-ferrospinels, RSC Adv., 5 (2015) 37925.

[81]. R. S. Yadav, I. Kuřitka, J. Vilcakova, J. Havlica, L. Kalina, P. Urbánek, M. Machovsky, M. Masař, M. Holek, Influence of La^{3+} on Structural, Magnetic, Dielectric, Electrical and Modulus Spectroscopic Characteristics of Single Phase $CoFe_{2-x}La_xO_4$ Nanoparticles, Journal of Materials Science: Materials in Electronics 28 (2017) 9139 – 9154.

[82]. N. Sivakumar, A. Narayanasamy, N. Ponpandian, and G. Govindaraj, Grain size effect on the dielectric behavior of nanostructured $Ni_{0.5}Zn_{0.5}Fe_2O_4$, J. Appl. Phys. 101 (2007) 084116.

[83]. N. Ponpandian and A. Narayanasamy, Influence of grain size and structural changes on the electrical properties of nanocrystalline zinc ferrite, J. Appl. Phys. 92 (2002) 2770.

[84]. A. Shukla, R.N.P. Choudhary, Impedance and modulus spectroscopy characterization of La^{+3}/Mn^{+4} modified $PbTiO_3$ nanoceramics, Current Applied Physics 11 (2011) 414-422.

[85]. M. M. Costa, G. F. M. Pires Jr., A. J. Terezo, M. P. F. Graça, and A. S. B. Sombra, Impedance and modulus studies of magnetic ceramic oxide $Ba_2Co_2Fe_{12}O_{22}$ (Co_2Y) doped with Bi_2O_3, Journal of Applied Physics 110 (2011) 034107.

[86]. D. G. Chen, X. G. Tang, Q. X. Liu, Y. P. Jiang, C. B. Ma, and R. Li, Impedance response and dielectric relaxation in co-precipitation derived ferrite (Ni,Zn)Fe_2O_4 ceramics, Journal of Applied Physics 113 (2013) 214110.

[87]. R. S. Yadav, I. Kuřitka, J. Vilcakova, J. Havlica, J. Masilko, L. Kalina, J. Tkacz, V. Enev, M. Hajdúchová, Structural, magnetic, dielectric, and electrical properties of $NiFe_2O_4$ spinel ferrite nanoparticles prepared by honey-mediated sol-gel combustion, Journal of Physics and Chemistry of Solids 107 (2017) 150–161.

[88]. R. S. Yadav, I. Kuřitka, J. Vilcakova, P. Urbanek, M. Machovsky, M. Masar, M. Holek, Structural, magnetic, optical, dielectric, electrical and modulus spectroscopic characteristics of $ZnFe_2O_4$ spinel ferrite nanoparticles synthesized via honey-mediated sol-gel combustion method, Journal of Physics and Chemistry of Solids 110 (2017) 87-99.

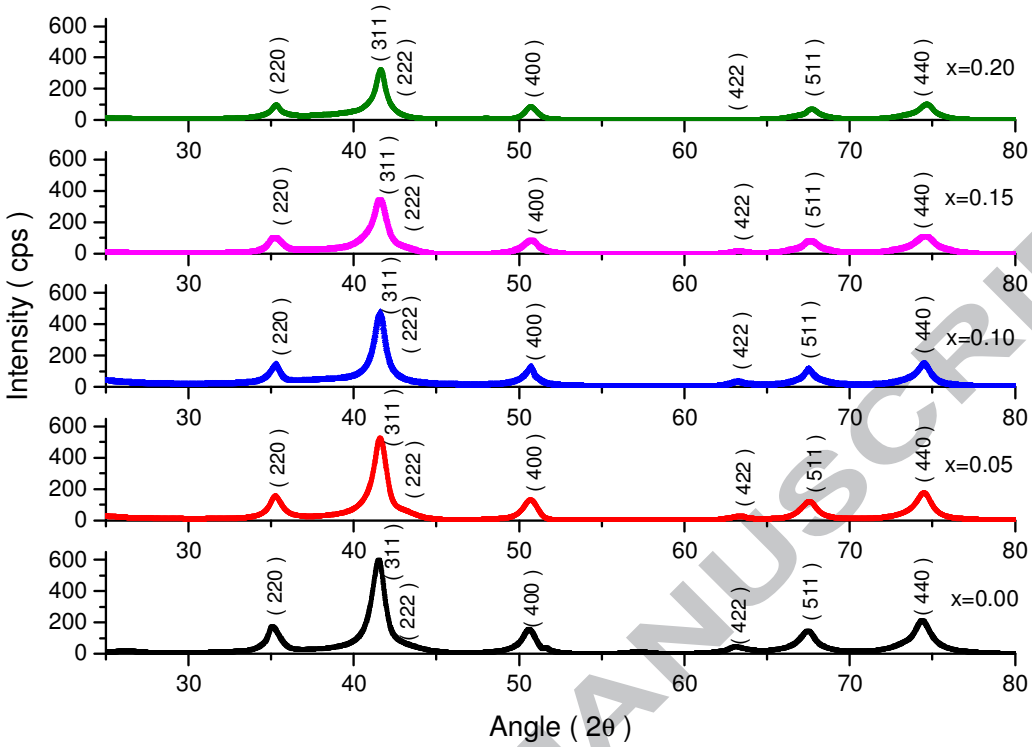

Fig. 1: X-ray diffraction patterns of $CoFe_{2-x}Gd_xO_4$ (x = 0.00, 0.05, 0.10, 0.15, 0.20) nanoparticles synthesized by sonochemical method.

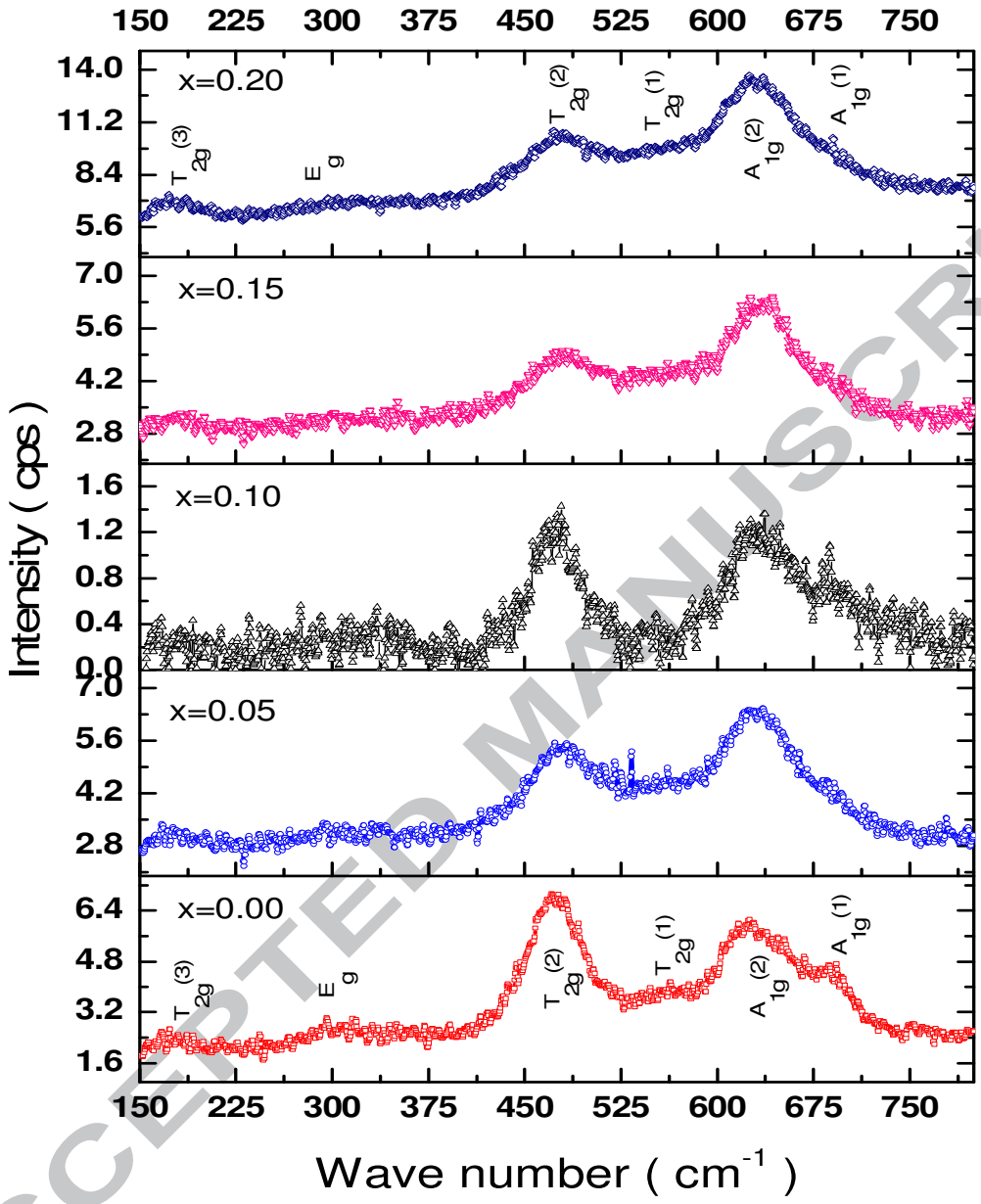

Fig. 2: Raman spectra of $CoFe_{2-x}Gd_xO_4$ (x=0.00, 0.05, 0.10, 0.15, 0.20) nanoparticles.

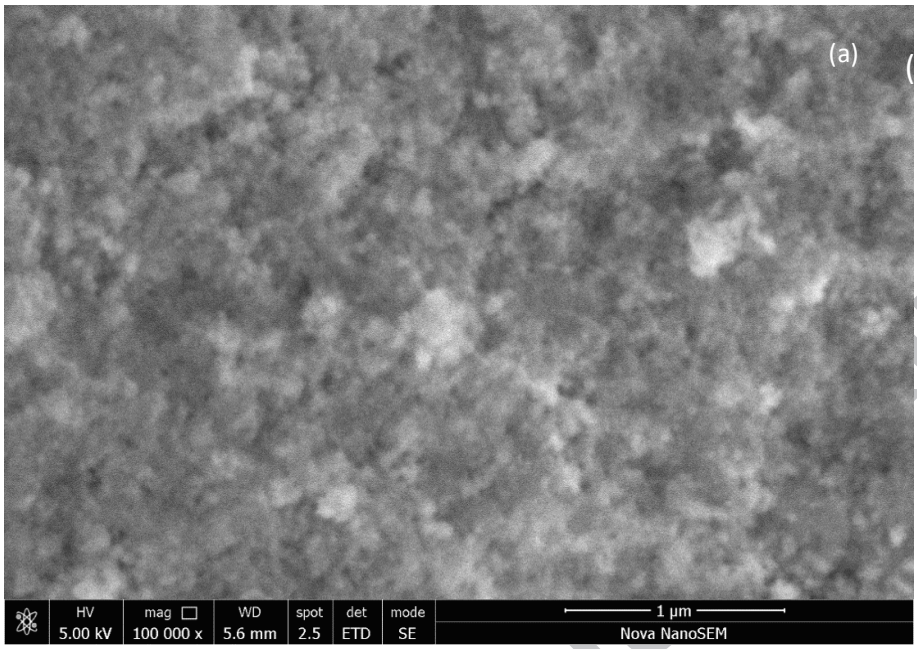

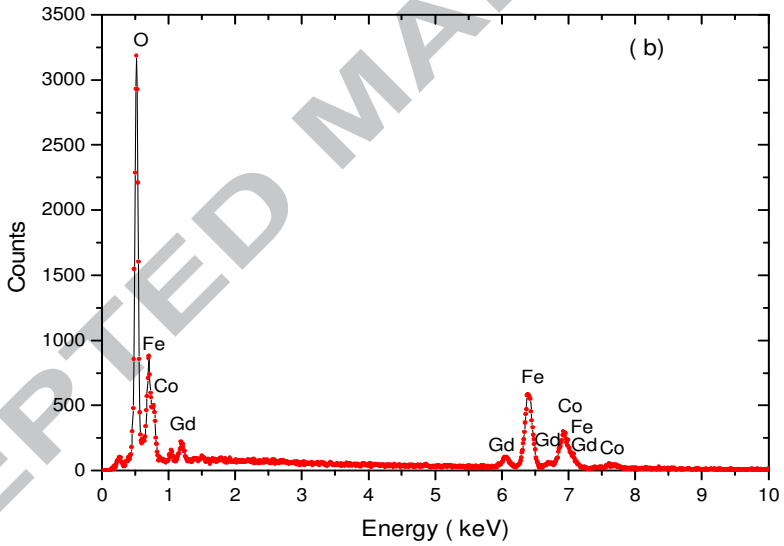

Fig. 3: (a) Scanning Electron Microscopy Image of $CoFe_{2-x}Gd_xO_4$ (x=0.20) nanoparticles synthesized by Sonochemical method. **(b)** EDX image of $CoFe_{2-x}Gd_xO_4$ (x=0.20) nanoparticles.

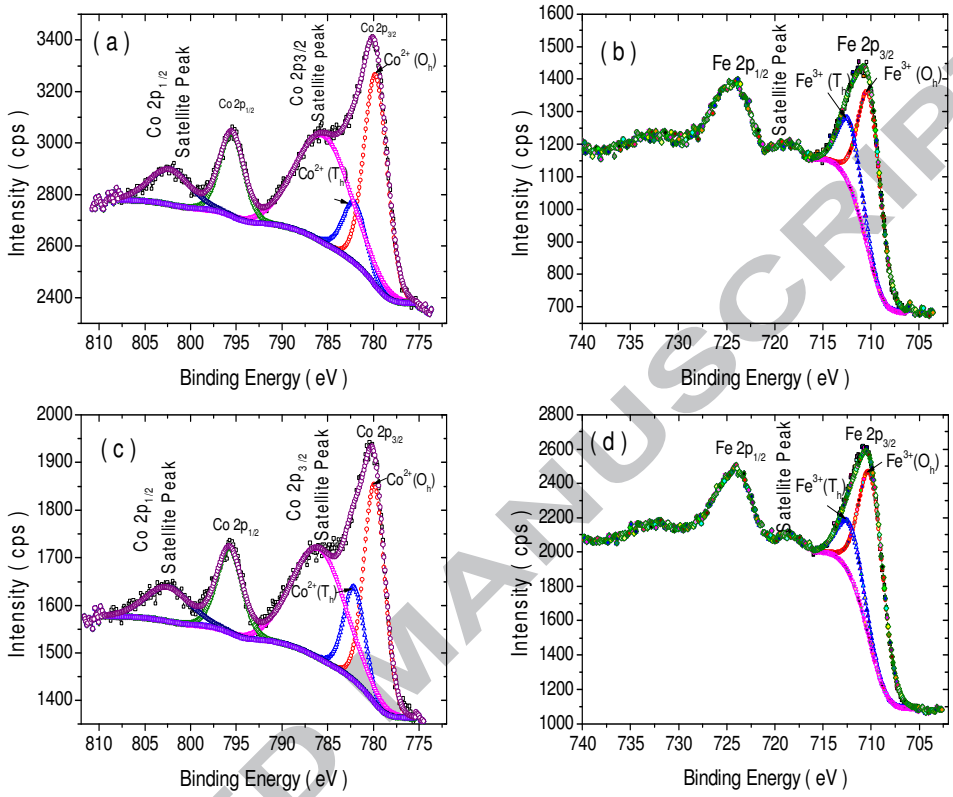

Fig. 4: X-ray photoelectron spectra of (a & b) $CoFe_{2-x}Gd_xO_4$ (x=0.10) nanoparticles and (c & d) $CoFe_{2-x}Gd_xO_4$ (x=0.20) nanoparticles.

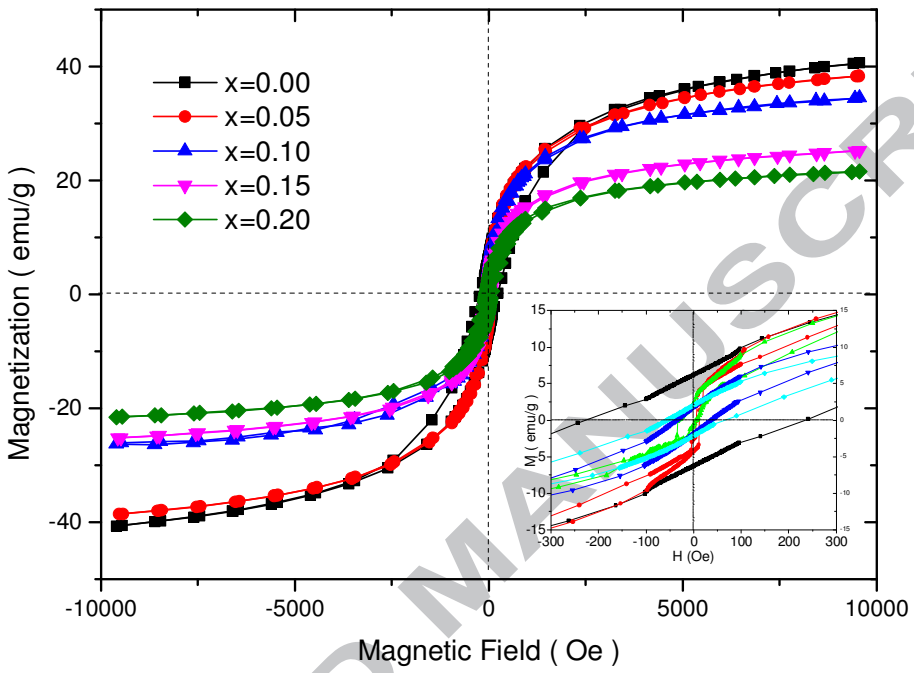

Fig. 5: Magnetic hysteresis curves of $CoFe_{2-x}Gd_xO_4$ (x=0.00, 0.05, 0.10, 0.15, 0.20) nanoparticles synthesized by sonochemical method. Inset is enlarge view of hysteresis curves.

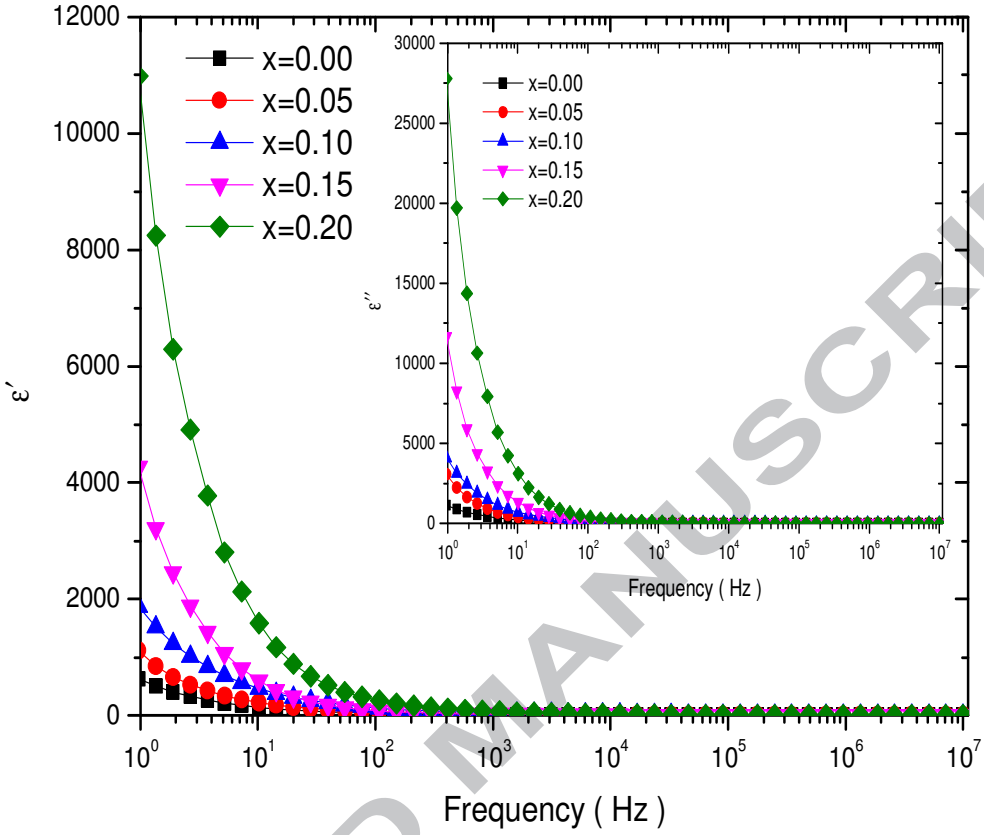

Fig. 6: Frequency dependence real part of dielectric constant (ε') for $CoFe_{2-x}Gd_xO_4$ (x=0.00, 0.05, 0.10, 0.15, 0.20) nanoparticles. Inset shows frequency dependence imaginary part of dielectric constant (ε'').

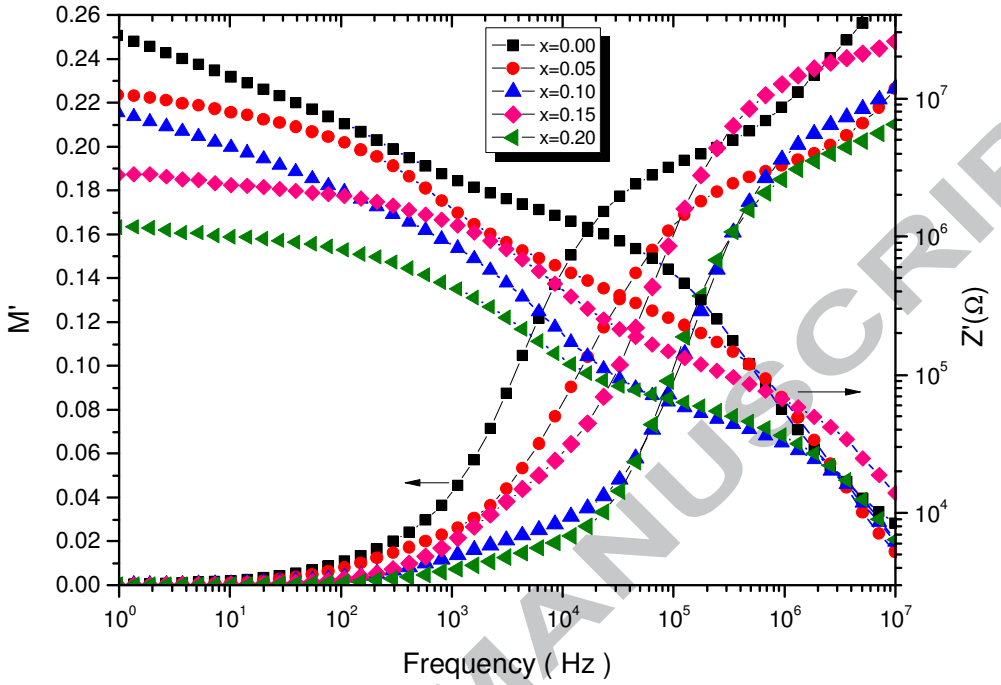

Fig. 7: Variation of real part of impedance (Z') and modulus (M') of $CoFe_{2-x}Gd_xO_4$ (x=0.00, 0.05, 0.10, 0.15, 0.20) nanoparticles synthesized by sonochemical method.

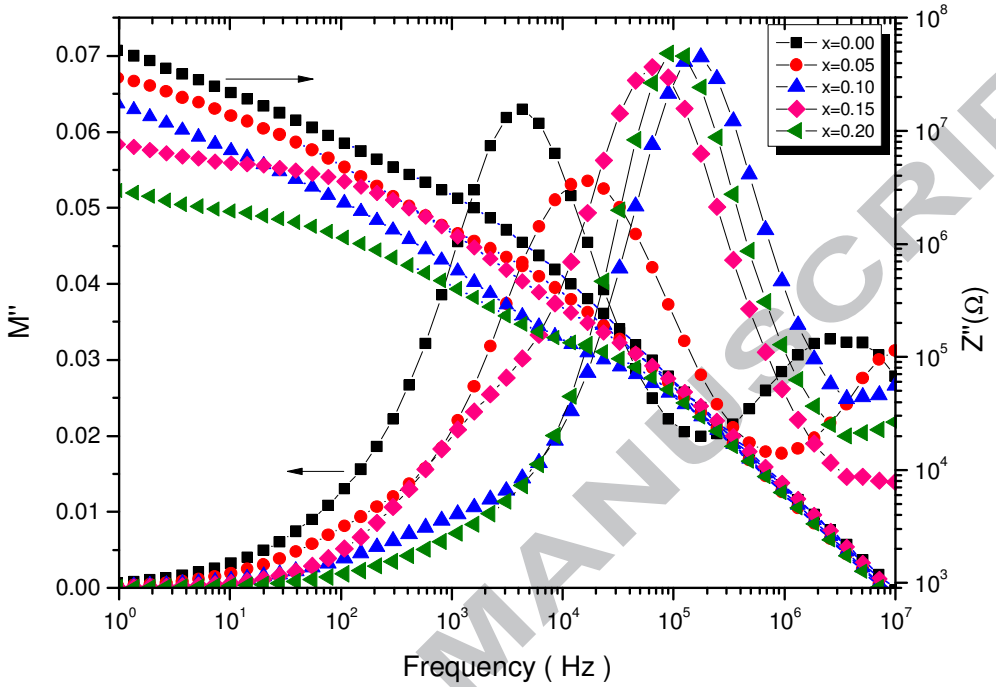

Fig. 8: Variation of imaginary part of impedance (Z'') and modulus (M'') of $CoFe_{2-x}Gd_xO_4$ (x=0.00, 0.05, 0.10, 0.15, 0.20) nanoparticles synthesized by sonochemical method.

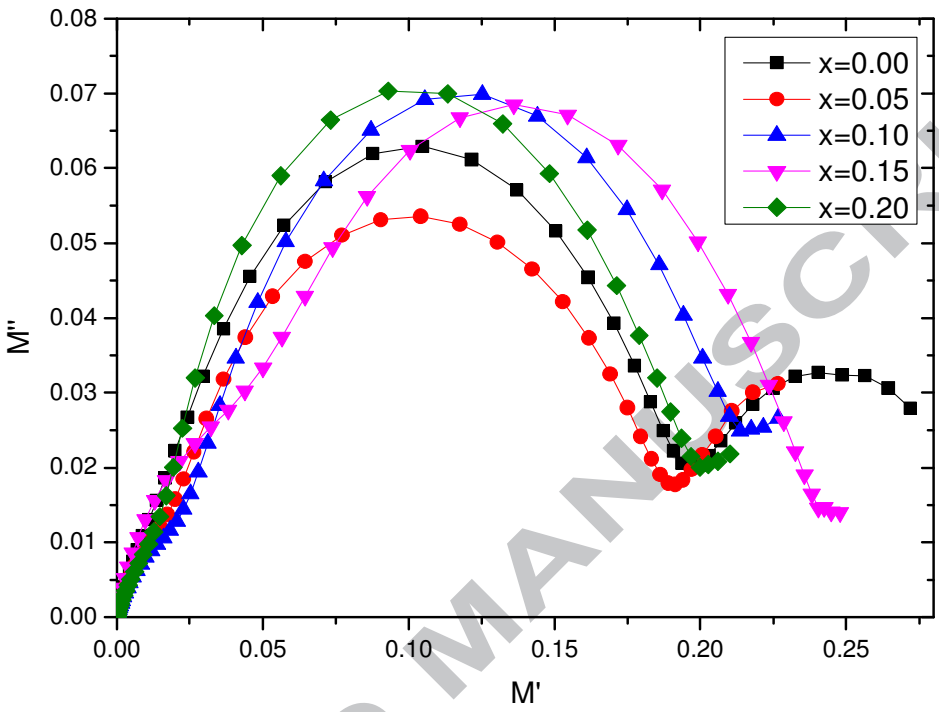

Fig. 9: Cole-Cole plot for $CoFe_{2-x}Gd_xO_4$ (x=0.00, 0.05, 0.10, 0.15, 0.20) nanoparticles synthesized by sonochemical method.

Table 1: Crystallite size (D), lattice constant (a), x-ray density (d_x), FTIR modes (v_1, v_2) and force constant (F_T and F_B) for $CoFe_{2-x}Gd_xO_4$ (x=0.00, 0.05, 0.10, 0.15, 0.20) nanoparticles.

x	D (nm)	a (Å)	d_x (g/cm^3)	v_1 (cm^{-1})	v_2 (cm^{-1})	$F_T x10^2$(N/m)	$F_B x10^2$(N/m)
0.00	9.2	8.3752	5.305	548	343	2.20	0.86
0.05	9.0	8.3643	5.441	556	348	2.27	0.88
0.10	8.8	8.3633	5.558	559	344	2.29	0.87
0.15	8.0	8.3557	5.689	566	357	2.34	0.93
0.20	7.6	8.3470	5.822	570	355	2.38	0.92

Table 2: The variation of bond length between cation-anion (p, q, r, s) and cation-cation (b, c, d, e, f) with Gd^{3+} concentration (x) for $CoFe_{2-x}Gd_xO_4$ (x=0.00, 0.05, 0.10, 0.15, 0.20) nanoparticles**.**

x	p (Å)	q (Å)	r (Å)	s (Å)	b (Å)	c (Å)	d (Å)	e (Å)	f (Å)
0.00	2.0435	1.9003	3.6388	3.6554	2.9606	3.4722	3.6265	5.4397	5.1287
0.05	2.0408	1.8978	3.6341	3.6507	2.9568	3.4676	3.6217	5.4326	5.1221
0.10	2.0406	1.8976	3.6336	3.6503	2.9564	3.4672	3.6213	5.4319	5.1215
0.15	2.0387	1.8958	3.6303	3.6469	2.9537	3.4641	3.6180	5.4270	5.1168
0.20	2.0366	1.8938	3.6265	3.6432	2.9506	3.4604	3.6143	5.4214	5.1115

Table 3: The variation of bond angles (θ_1, θ_2, θ_3, θ_4, and θ_5) between cations and cation-anion with Gd^{3+} concentration (x) for $CoFe_{2-x}Gd_xO_4$ (x=0.00, 0.05, 0.10, 0.15, 0.20) nanoparticles**.**

x	θ_1	θ_2	θ_3	θ_4	θ_5
0.00	123.3439	144.9380	92.8359	125.9243	74.4787
0.05	123.3418	144.9382	92.8360	125.9244	74.4786
0.10	123.3414	144.9375	92.8354	125.9240	74.4787
0.15	123.3413	144.9374	92.8354	125.9240	74.4787
0.20	123.3414	144.9375	92.8354	125.9239	74.4786

Table 4: Raman modes of $CoFe_{2-x}Gd_xO_4$ (x=0.00, 0.05, 0.10, 0.15, 0.20) nanoparticles.

x	Raman Peak (cm^{-1})					
	$A_{1g}(1)$	$A_{1g}(2)$	$T_{2g}(1)$	$T_{2g}(2)$	E_g	$T_{2g}(3)$
0.00	687	624	561	472	299	180
0.05	687	626	559	475	295	176
0.10	689	628	548	477	290	176
0.15	689	633	544	479	286	173
0.20	689	635	542	479	284	171

Table 5: XPS results for $CoFe_{2-x}Gd_xO_4$ (x = 0.10 & 0.20) nanoparticles synthesized by sonochemical method.

Sample	Spectrum	B.E.(eV)	Assignment	Atomic Percentage (%)
$CoFe_{2-x}Gd_xO_4$ (x=0.10)	Co $2p_{3/2}$	779.7	Octahedral Co^{2+}	78
		782.1	Tetrahedral Co^{2+}	22
	Fe $2p_{3/2}$	709.9	Octahedral Fe^{3+}	71
		712.7	Tetrahedral Fe^{3+}	29
$CoFe_{2-x}Gd_xO_4$ (x=0.20)	Co $2p_{3/2}$	779.9	Octahedral Co^{2+}	70
		782.1	Tetrahedral Co^{2+}	30
	Fe $2p_{3/2}$	710.1	Octahedral Fe^{3+}	77
		712.2	Tetrahedral Fe^{3+}	23

Table 6 : Crystallite size D (nm), M_s(emu/g), H_c(Oe), M_r(emu/g), M_r/M_s, K(erg.Oe/g), $\eta_B(\mu_B)$, $\alpha_{yk}(^O)$, and μ_i for $CoFe_{2-x}Gd_xO_4$ (x=0.00, 0.05, 0.10, 0.15, 0.20) nanoparticles.

x	D (nm)	M_s(emu/g)	H_c(Oe)	M_r(emu/g)	M_r/M_s	$Kx10^3$ (erg.Oe/g)	$\eta_B(\mu_B)$	$\alpha_{yk}(^O)$	μ_i
0.00	9.2	40.19	234.32	6.27	0.150	9.81	1.68	0	1.514
0.05	9.0	38.24	12.60	2.46	0.064	0.50	1.64	0	26.321
0.10	8.8	34.81	27.31	2.51	0.072	0.99	1.53	$8^o 53'$	10.771
0.15	8.0	25.04	33.36	1.82	0.073	0.87	1.12	$29^o 11'$	5.765
0.20	7.6	21.58	68.62	2.11	0.097	1.54	0.98	$36^o 34'$	2.298

Table 7 : Electrical parameters : ϵ', tanδ, σ , τ_{gb}, C_{gb} , R_{gb} for $CoFe_{2-x}Gd_xO_4$ (x=0.00, 0.05, 0.10, 0.15, 0.20) nanoparticles**.**

x	ϵ'		tanδ		σ $X10^{-9}$ (S/cm)		τ_{gb}(μs)	C_{gb}(pF)	R_{gb}(KΩ)
	100 Hz	**1kHz**	**100 Hz**	**1kHz**	**100 Hz**	**1kHz**			
0.00	39.6	11.9	1.2	1.0	2.6	6.5	36.0	70.3	513.0
0.05	65.1	23.7	1.0	0.8	3.5	10.8	9.2	82.0	112.0
0.10	134.6	50.8	1.1	0.7	8.1	20.0	0.9	63.3	14.5
0.15	88.6	25.9	1.8	1.0	8.8	13.9	2.3	65.2	35.6
0.20	277.6	75.5	1.5	0.9	20.2	40.1	1.5	63.3	23.1

Graphical Abstract

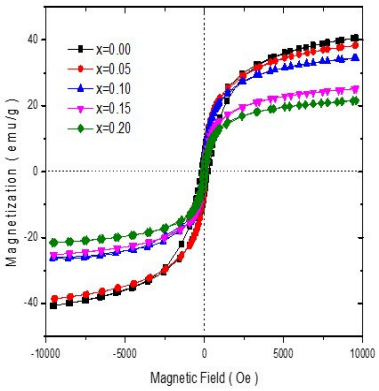

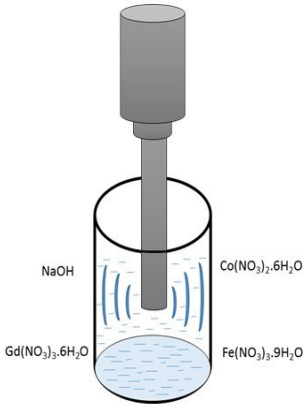

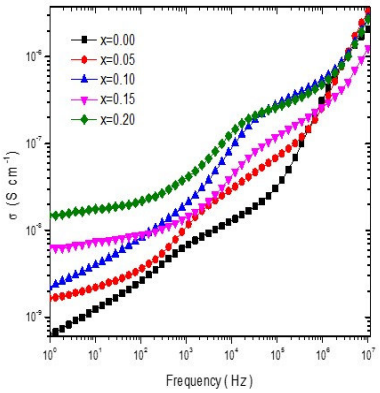

Highlights

- $CoFe_{2-x}Gd_xO_4$ (x = 0.00, 0.05, 0.10, 0.15, 0.20) nanoparticles synthesized by sonochemical method.
- Sonochemical synthesis is favourable to form highly crystalline single spinel crystal phase nanoparticles.
- Variation in magnetic properties with Gd^{3+} substitution in $CoFe_2O_4$ nanoparticles.
- Enhanced dielectric constant and ac conductivity.